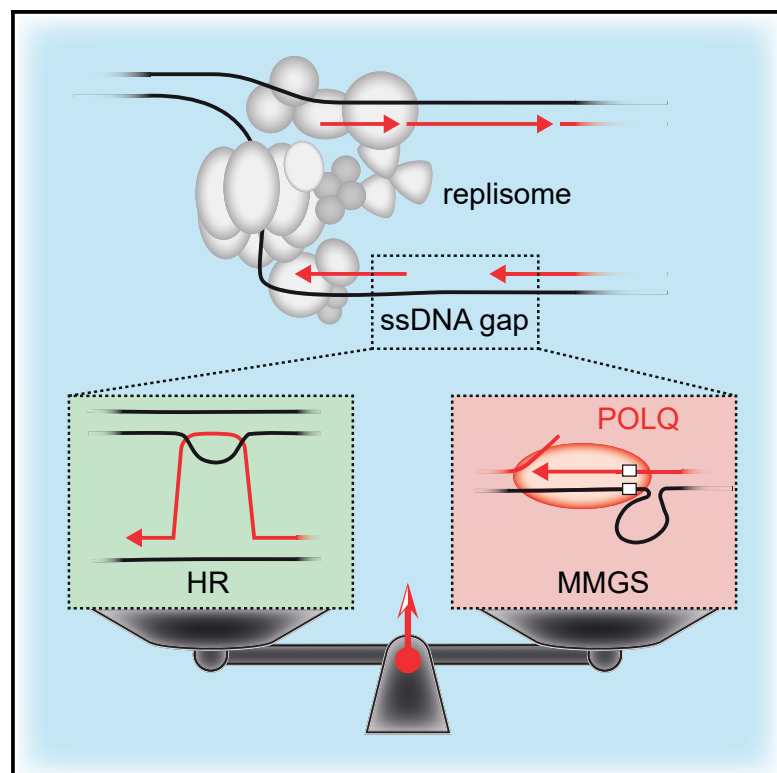


POLQ seals post-replicative ssDNA gaps to maintain genome stability in BRCA-deficient cancer cells

Graphical abstract



Authors

Ondrej Belan, Marie Sebald, Marek Adamowicz, ..., Stephen C. West, David S. Rueda, Simon J. Boulton

Correspondence

simon.boulton@crick.ac.uk

In brief

Belan et al. exploit genetic, biochemical, and single-molecule approaches to reveal POLQ loss or inhibition leads to accumulation of post-replicative ssDNA gaps in BRCA1/2-deficient cells, which is further exacerbated by treatment with PARP inhibitors. This provides mechanistic insight into synthetic killing of HR-deficient cancers by POLQ inhibitors.

Highlights

- BRCA-deficient cells accumulate post-replicative gaps following POLQ loss or inhibition
- PARP inhibitors exacerbate ssDNA gap accumulation in BRCA-deficient POLQ KO cells
- POLQ strips RPA to allow for DNA synthesis across a model ssDNA gap *in vitro*
- POLQ catalyzes microhomology-mediated gap skipping (MMGS) *in vitro*



Article

POLQ seals post-replicative ssDNA gaps to maintain genome stability in BRCA-deficient cancer cells

Ondrej Belan,¹ Marie Sebald,² Marek Adamowicz,¹ Roopesh Anand,¹ Aleksandra Vancevska,¹ Joana Neves,⁶ Vera Grinkevich,⁶ Graeme Hewitt,^{1,8} Sandra Segura-Bayona,¹ Roberto Bellelli,³ Helen M.R. Robinson,⁶ Geoff S. Higgins,⁷ Graeme C.M. Smith,⁶ Stephen C. West,² David S. Rueda,^{4,5} and Simon J. Boulton^{1,6,9,*}

¹DSB Repair Metabolism Laboratory, The Francis Crick Institute, London NW1 1AT, UK

²DNA Recombination and Repair Laboratory, The Francis Crick Institute, London NW1 1AT, UK

³Centre for Cancer Cell and Molecular Biology, Barts Cancer Institute, Queen Mary University of London, London EC1M 6BQ, UK

⁴Department of Infectious Disease, Faculty of Medicine, Imperial College London, London W12 0NN, UK

⁵Single Molecule Imaging Group, MRC-London Institute of Medical Sciences, London W12 0NN, UK

⁶Artios Pharma Ltd., B940 Babraham Research Campus, Cambridge CB22 3FH, UK

⁷Medical Research Council Oxford Institute for Radiation Oncology, University of Oxford, Old Road Campus Research Building, Roosevelt Drive, Oxford OX3 7DQ, UK

⁸Present address: School of Cancer & Pharmaceutical Sciences, King's College London, London SE1 9RT, UK

⁹Lead contact

*Correspondence: simon.boulton@crick.ac.uk

<https://doi.org/10.1016/j.molcel.2022.11.008>

SUMMARY

POLQ is a key effector of DSB repair by microhomology-mediated end-joining (MMEJ) and is overexpressed in many cancers. POLQ inhibitors confer synthetic lethality in HR and Shieldin-deficient cancer cells, which has been proposed to reflect a critical dependence on the DSB repair pathway by MMEJ. Whether POLQ also operates independent of MMEJ remains unexplored. Here, we show that POLQ-deficient cells accumulate post-replicative ssDNA gaps upon BRCA1/2 loss or PARP inhibitor treatment. Biochemically, cooperation between POLQ helicase and polymerase activities promotes RPA displacement and ssDNA-gap fill-in, respectively. POLQ is also capable of microhomology-mediated gap skipping (MMGS), which generates deletions during gap repair that resemble the genomic scars prevalent in POLQ overexpressing cancers. Our findings implicate POLQ in mutagenic post-replicative gap sealing, which could drive genome evolution in cancer and whose loss places a critical dependency on HR for gap protection and repair and cellular viability.

INTRODUCTION

DNA double-strand breaks (DSBs) are among the most toxic genomic lesions. To counter DSB formation, our cells have evolved multiple pathways to repair these lesions. Homologous recombination (HR) is a DSB repair pathway restricted to S and G2 phases of the cell cycle.¹ It utilizes an intact sister chromatid as a template for DNA synthesis to restore the broken chromosome in a largely error-free manner. End-joining pathways—non-homologous end-joining (NHEJ) and microhomology-mediated end-joining (MMEJ)—can operate throughout the cell cycle and mend the break by joining the free DNA ends together. MMEJ utilizes small homologies (1–4 nt) present at nucleolytically resected DNA ends, which generates specific DNA scars; small deletions containing microhomology at the breakpoint junction.² DNA polymerase theta (POLQ) is a bona fide MMEJ factor that is overexpressed in many cancers,³ including, but not limited to, HR and shieldin-deficient cancers.^{4,5} Evidence suggests that

POLQ is responsible for the accumulation of genomic scars harboring microhomologies in cancers.^{2,6,7} Importantly, genetic ablation of POLQ confers specific cell killing (synthetic lethality) in HR-deficient and shieldin-deficient cancers.^{4,7} This observation implies that POLQ acts in parallel to HR and NHEJ to promote cell survival.

POLQ is a large protein consisting of a helicase (HD) and polymerase domain (PD) joined by a disordered central domain. Both catalytic domains are important for POLQ-mediated MMEJ and deletion of either of these domains confers synthetic lethality with HR-deficiency.⁸ It has been suggested that the helicase domain of POLQ is important for the removal of replication protein A (RPA) from microhomology-containing single-stranded DNA (ssDNA) strands.⁸ RPA binds ssDNA with sub-nanomolar affinity and is important for protection of intrinsically fragile ssDNA¹; however, RPA binding to ssDNA presents a barrier to many physiologically relevant DNA transactions including MMEJ. 3' ends of annealed ssDNA strands are extended by the PD of POLQ.⁸ Further processing by other



factors, such as FEN1,⁹ LIG1,¹⁰ and LIG3^{11,12} may then allow for flap cleavage, strand ligation, and completion of the MMEJ reaction.

Recently, inhibitors against both POLQ helicase and POLQ polymerase have been developed.^{5,13} These POLQ inhibitors (POLQi) confer specific killing of BRCA-deficient cells and synergize with the poly(ADP-ribose) polymerase (PARP) inhibitor (PARPi), olaparib, which is the first clinically approved compound for specific treatment of BRCA-deficient tumors. Importantly, POLQi also circumvents common mechanisms of PARPi resistance, such as loss of shieldin complex components, which counteracts the processing of DSB break ends.^{14–18} These findings underscore the potential of POLQi as second-generation compounds for the treatment of BRCA-deficient tumors, including those that have acquired PARPi resistance.

Despite recent advancements, the mechanism of synthetic lethality between POLQ inhibition and BRCA-deficiency is not fully understood. It is currently unclear why the combination of POLQi and PARPi is synergistic, as PARP1 acts upstream of POLQ in MMEJ repair of DSBs¹⁹ and is believed to be important for POLQ recruitment to sites of irradiation.⁷ PARPi can also cause toxicity through inhibition of replication fork (RF) reversal^{20,21} and accelerating the speed of RFs,²² which is accompanied by ssDNA gap accumulation behind the replisome.²³ These ssDNA gaps are repaired by HR under physiological conditions. However, in BRCA-deficient cells, ssDNA gaps extensively accumulate, which could drive genome instability and cell death.^{23,24} Whether POLQ also acts to seal post-replicative ssDNA gaps is not understood.

Here, we show that POLQ-deficient cells treated with olaparib or depleted of BRCA2 exhibit increased levels of ssDNA in replicating cells, which we show is due to the accumulation of ssDNA gaps behind RFs. The extent of post-replicative ssDNA gap formation is most severe following BRCA2 depletion in combination with PARPi. We also show that POLQi causes post-replicative ssDNA gap accumulation in BRCA1 hypomorphs in a manner that correlates with cellular viability. Through biochemical reconstitution, we find that POLQ is a potent ssDNA gap filling enzyme. This requires RPA stripping by POLQ helicase, DNA synthesis by POLQ polymerase, and gap sealing by FEN1 and LIG1. We further discover that POLQ can promote microhomology-mediated gap skipping (MMGS) by annealing microhomologies present at the 3' ssDNA (single-stranded-double-stranded DNA) junction and within the ssDNA gap, resulting in deletion of intervening sequences. Taken together, our findings reveal an unappreciated role for POLQ in mutagenic sealing of post-replicative ssDNA gaps, which provides an alternative explanation for the synthetic lethality between POLQ and HR-deficiency.

RESULTS

POLQ prevents the accumulation of ssDNA in replicating cells

Previous studies have observed enrichment of POLQ on replicating chromatin.²⁵ POLQ loss is also synthetic lethal with FANCD2 loss, which is required for replication-coupled repair

of inter-strand crosslinks.⁴ These data raised the possibility that POLQ may function in S-phase cells, potentially during perturbed DNA replication. To explore this, we generated isogenic wild-type and POLQ knockouts (KOs) in diploid eHAP (haploid engineered HAP1) cells using CRISPR-Cas9 (Figure 1A). Both POLQ KO clones were deficient for MMEJ using an extrachromosomal MMEJ reporter construct (Figure 1B)¹³ and exhibited synthetic lethality upon BRCA2 depletion (Figures 1C and S1A).^{4,7} We observed increased micronuclei in POLQ KO cells following BRCA2 depletion (Figure 1C), which was also observed following POLQi-treatment in BRCA-deficient cancer cells¹³ and in erythrocytes in POLQ-deficient mice upon radiation- or mitomycin C-induced treatment.²⁶

Since micronucleation is a hallmark of replication stress, we examined POLQ KO cells for ssDNA accumulation by native 5-chloro-2'-deoxyuridine (CldU) and proliferating cell nuclear antigen (PCNA, replication marker) immunofluorescence in asynchronously growing cultures. We observed a strong increase of ssDNA (CldU) staining in POLQ KO cells following BRCA2 depletion (Figures 1D and 1E). Since ssDNA is often bound by RAD51 to engage HR and protect ssDNA from nucleolytic degradation, we also monitored RAD51 focus formation in POLQ KO cells. We observed a significant increase in RAD51 foci formation in EdU-positive cells, which label replicating cells within the population (Figures S1B and S1C). RAD51 is recruited to and loaded onto ssDNA by BRCA2.²⁷ As such, BRCA2 depletion eliminated the elevated levels of RAD51 foci in POLQ KO cells. Combined loss of BRCA2 and POLQ also resulted in increased 53BP1 foci, particularly in the EdU-positive cell population (Figures S1D and S1E), similarly to previous reports.²⁸ Collectively, this implies ssDNA arises during replication in the absence of POLQ and RAD51 loading by BRCA2.

POLQ seals post-replicative ssDNA gaps

To examine the underlying cause of elevated ssDNA in POLQ-deficient cells, we employed the DNA fiber assay. Using this approach, we considered the possibility that POLQ could either prevent the accumulation of stalled, collapsed, or broken RFs, as has been reported for HR proteins,^{29,30} or prevent formation of post-replicative ssDNA gaps (Figure 1F). To this end, we pulse-labeled active RFs with CldU and then IdU (5-iodo-2'-deoxyuridine) nucleotide analogs and visualized the labeled RFs by immunofluorescence (Figures 1G and 1H). We did not observe a significant fork slowing in POLQ KO cells, with or without BRCA2 depletion (Figure 1I). Consistent with previous studies,^{29,30} increased fork asymmetry was observed upon BRCA2 depletion. This indicates increased fork stalling or collapse. However, only a modest increase in fork asymmetry was observed on POLQ loss in BRCA2-depleted cells (Figure 1J).

Since HR is known to play a role in the repair of post-replicative ssDNA gaps, we also consider the possibility that RPA-ssDNA gaps might accumulate behind the fork in POLQ KO cells \pm BRCA2.^{23,30–32} To test this possibility, we subjected the CldU and IdU-labeled replication tracts to an S1 nuclease digestion step (Figures 1G and 1H). If ssDNA gaps are present behind the replisome, S1 nuclease treatment will result in selective

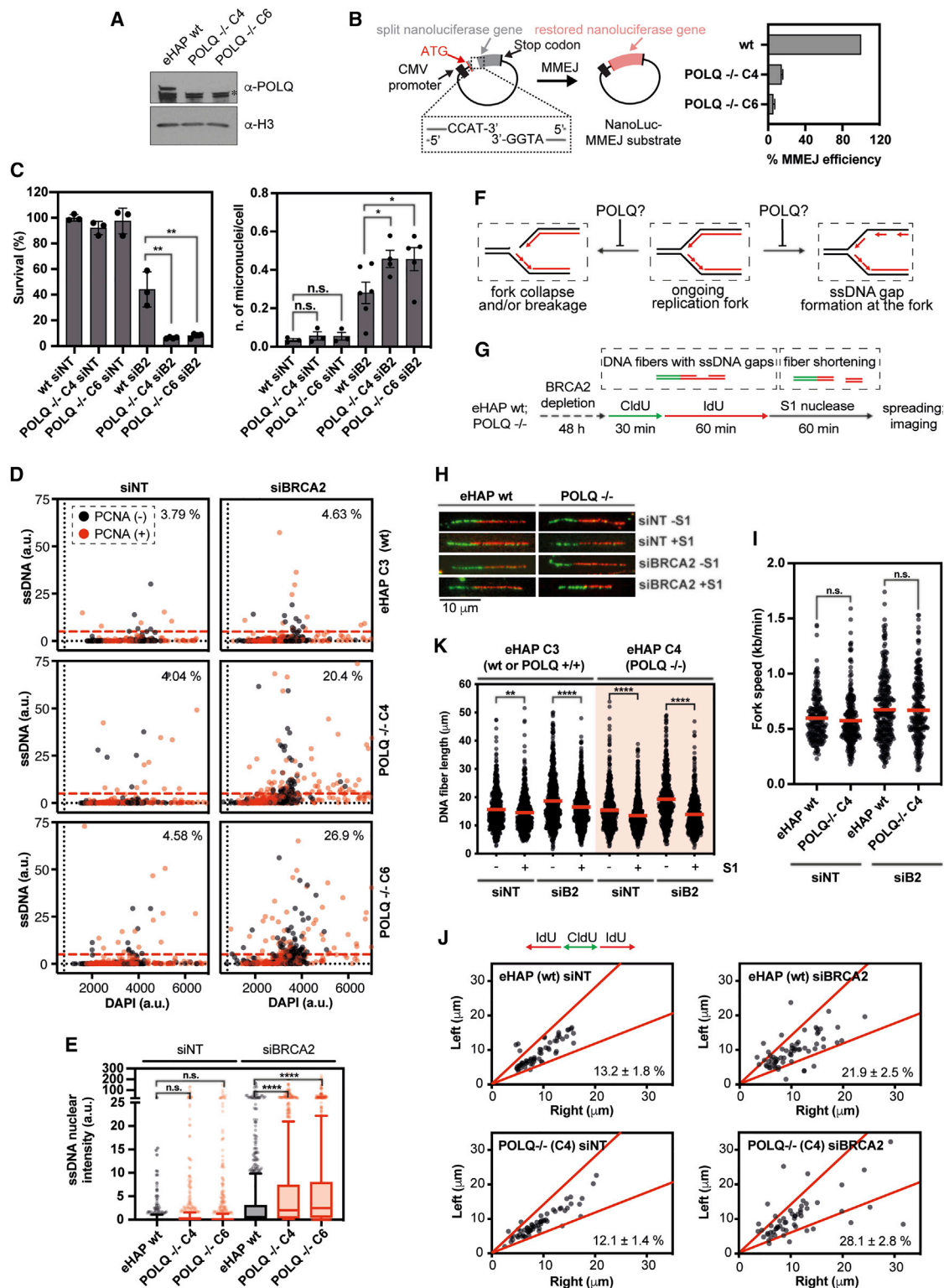


Figure 1. POLQ seals post-replicative ssDNA gaps in BRCA2-depleted cells

(A) Immunoblot of WCEs in POLQ +/+ and two independently generated POLQ -/- clones (clones 4 and 6), probed for POLQ.

(B) Left: schematic describing MMEJ reporter assay. Right: MMEJ efficiency quantification. Bars present mean \pm SD normalized to mean of POLQ +/+ eHAP cells (n = 2).

(legend continued on next page)

incision of the ssDNA gaps, shortening the replication tract length.³³ Although replication tracts remained mostly resistant to S1 nuclease treatment in BRCA2 or POLQ-deficient cell lines, combined BRCA2/POLQ-deficiency resulted in significant replication tract shortening upon S1 treatment (Figure 1K). This indicates that post-replicative ssDNA gaps accumulate in HR-deficient POLQ KO cells.

PARPi-mediated fork acceleration exacerbates ssDNA gap accumulation in POLQ-deficient cancer cells upon loss of HR

We recently reported that combining POLQ (ART558) and PARP inhibitors confer synergistic killing of HR-deficient cells.^{5,13} Since PARP inhibitors prevent RF reversal²⁰ and result in ssDNA gap formation in BRCA-deficient cells,²³ we considered the possibility that the synergistic effect of combining POLQ deficiency and PARP inhibitors may reflect an accumulation of post-replicative ssDNA gaps. To this end, we treated non-targeting and BRCA2-depleted POLQ KOs with increasing dose of PARPi (olaparib) and observed moderate sensitivity of POLQ KO cells to PARPi and additive killing of BRCA2-depleted POLQ KO cells (Figure 2A). These results were confirmed in clonogenic survival assays (Figures S1F and S1G). To examine ssDNA accumulation in these cells, we monitored native CldU staining in PCNA-positive cells following PARPi treatment (Figure 2B). We observed an increased proportion of cells with ssDNA signal (Figure 2B) and overall ssDNA intensity (Figure 2C) across all conditions, but particularly in BRCA2 and BRCA2/POLQ-deficient cells. Next, we employed the DNA fiber assay combined with S1 nuclease treatment to monitor fork dynamics and post-replicative ssDNA gap formation (Figure 2D). We treated cells of the indicated genotype for 24 h with 0.5 μ M olaparib, the minimal effective dose required to observe S1 sensitization in HR-deficient cells.²³ We observed increased fork speeds on olaparib treatment even in wild-type (WT) cells, as was previously reported for prolonged (24 h) treatments,^{22,23} which was further increased upon BRCA2 depletion (Figure 2E). On PARPi treatment, we also observed only a subtle additional increase in fork speed in BRCA2-depleted POLQ KOs compared with BRCA2-depleted

WT cells (Figure 2E). This finding reinforces the notion that POLQ plays a minor role in regulating fork speed when BRCA2 is depleted and PARP is inhibited.

Consistent with previous work, we also observed a modest decrease in replication tract length upon S1 treatment in olaparib-treated BRCA2-depleted cells (Figure 2F). We further observed a significant replication track shortening on PARPi treatment in POLQ KO cells, but not in the WT controls (Figure 2F). Strikingly, replication track shortening was substantially increased in BRCA2-depleted POLQ KO cells on PARPi treatment. These data raised the possibility that POLQ seals post-replicative ssDNA gaps on PARPi treatment and/or following BRCA2 depletion. We note, however, that global ssDNA intensity levels in PARPi-treated BRCA2-depleted POLQ KOs (Figure 2C) do not completely correlate with replication tract shortening on S1 treatment (Figure 2F). This could reflect the lower specificity of the CldU staining assay compared with S1-coupled DNA fiber assay, which detects strictly post-replicative ssDNA structures. In CldU staining, the ssDNA signal may also reflect gaps in cells that passed through S-phase and accumulated in G2. Consistent with this, we observed an increase of ssDNA intensities in PCNA-negative cells in BRCA2-depleted POLQ KOs (Figures 1D and 2B). POLQ KO clones were mildly sensitive to olaparib (Figures 2A, S1F, and S1G), which is in line with the increased ssDNA signal (Figures 2B and 2C) and S1 sensitization (Figure 2F) in olaparib-treated POLQ KOs. Taken together, our results indicate that POLQ prevents post-replicative ssDNA gap accumulation induced by PARPi treatment, particularly in cells with HR-deficiency.

POLQi expose ssDNA gaps in PARPi-resistant SHLD-deficient BRCA1 hypomorphs

Acquired PARP inhibitor resistance is a common occurrence in HRD (homologous recombination-deficient) cancers in the clinic. Among several mechanisms, PARPi resistance is observed on the loss of any of the factors constituting the pro-NHEJ 53BP1-RIF1-shieldin complex (REV7, SHLD1, SHLD2, and SHLD3),^{14–18,34–36} which leads to DNA end resection and HR restoration in BRCA1 hypomorphs.³⁷ Importantly, unlike PARPi, POLQi induces killing of BRCA1 hypomorphs that have

(C) Left: survival in POLQ +/+ and POLQ –/– eHAP cells transfected with siBRCA2 measured using CellTiter-Glo. Bars present mean \pm SD normalized to mean of POLQ +/+ cells. Right: Quantification of number of micronuclei per primary nucleus from POLQ +/+ and POLQ –/– eHAP cells transfected with indicated siRNAs. Bar represents mean. Error bars indicate SEM. p values by Student's t test.

(D) Representative results of a single biological replicate of native CldU (ssDNA), PCNA, and DAPI staining of POLQ +/+ and POLQ –/– eHAP cells transfected with indicated siRNAs. Red line represents cutoff for calculation of ssDNA-positive fraction of cells indicated in the upper right corner.

(E) Quantification of global ssDNA intensity in total cell population. Boxplot graph displays median values with 10–90 percentile (N = 714–1,116 nuclei for each condition, n = 3 independent experiments). p values by Mann-Whitney test. The data presented correspond to the same dataset as data in Figure 2C.

(F) Schematic illustrating possible actions of POLQ at ongoing replication forks.

(G) Schematic illustrating DNA fiber protocol with or without S1 nuclease treatment for analysis of replication forks in POLQ +/+ and POLQ –/– eHAP cells transfected with the indicated siRNAs.

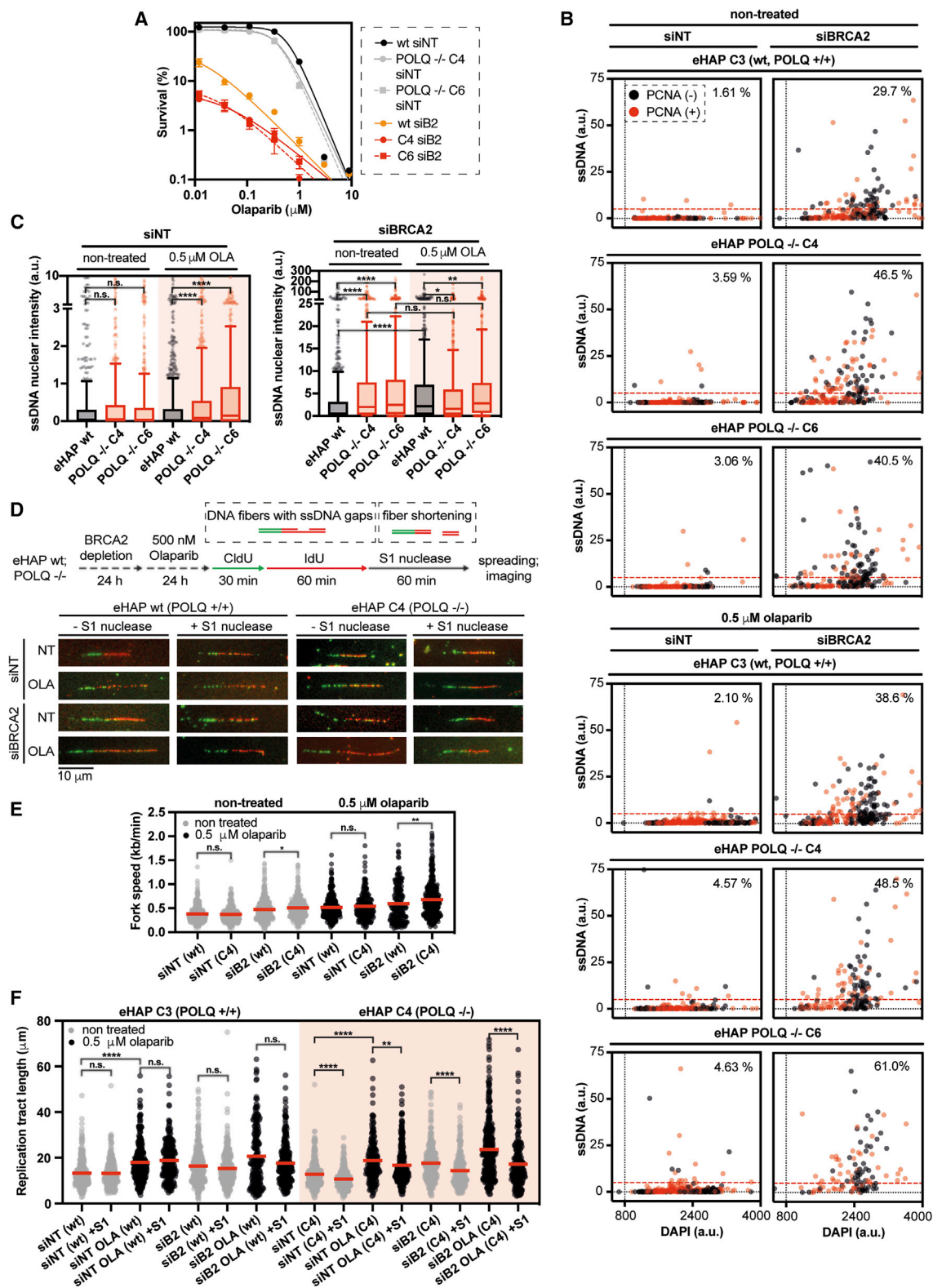
(H) Representative immunofluorescence images of stretched dual-stained DNA fibers from experiment in (G). Scale bars, 10 μ m.

(I) Measured fork rates in POLQ +/+ and POLQ –/– (clone 4, C4) eHAP cells transfected with the indicated siRNAs (N = 214–304 fibers for each condition, n = 2 replicates). Red lines represent mean. p values by Mann-Whitney test.

(J) Scatterplot of lengths of IdU DNA fiber tracts from the same replication origin in POLQ +/+ and POLQ –/– eHAP cells transfected with the indicated siRNAs (N = 55–64 fibers for each condition, n = 2 replicates).

(K) Measured length of individual dual-labeled DNA fibers in POLQ +/+ and POLQ –/– (clone 4, C4) eHAP cells transfected with the indicated siRNAs with or without S1 nuclease treatment. Red line represents mean (N = 470–829 fibers for each condition, n = 4 replicates). p values by Mann-Whitney test.

(A–K) n.s. p > 0.05; * p \leq 0.05; ** p \leq 0.01; *** p \leq 0.001; **** p \leq 0.0001.



(legend on next page)

lost shieldin.^{5,13} This suggests that POLQ could be employed to overcome certain mechanisms of PARPi resistance in HRD cancers. Similarly to error-free DSB repair restoration in 53BP1-RIF1-shieldin-deficient BRCA1 hypomorphs,³⁷ ssDNA gap exposure and fork speeding is also rescued.²³

We initially attempted depletion of BRCA1 in WT or POLQ KO eHAP cells. However, in contrast to BRCA2 depletion, we did not observe a strong synthetic lethality phenotype (Figure S2A) nor killing of the cells with olaparib (Figure S2B). This is reminiscent of a differential phenotype observed upon BRCA1 and BRCA2 KO induction in POLQ KO MEFs.²⁸ Given that rescue of PARPi sensitivity by loss of 53BP1-RIF1-shieldin complex is observable in BRCA1 hypomorphs,³⁷ rather than full KOs, we took advantage of previously established PARPi-sensitive BRCA1 hypomorph models to understand if ssDNA gaps may be re-exposed in PARPi-resistant cancer cell models on POLQ inhibition.

SUM149PT cells harboring a frameshift mutation at P724 of BRCA1 were co-transfected with *S.p.* Cas9 and crRNA (CRISPR RNA) targeting individual components of the 53BP1-RIF1-shieldin complex. PARPi-resistant cells were then selected by culturing in the presence of olaparib and talazoparib (Figure S2C). Gene KO was verified by western blotting (Figure S2D), sequencing, and/or phenotypic characterization. For the purpose of this study, we focused on the phenotypic characterization of SUM149PT^{BRCA1mut} parental cell line and SUM149PT^{BRCA1mut}/SHLD2 KO. As a control, the SUM149PT revertant cell line, which harbors a frameshift restoring ORF of BRCA1 was analyzed alongside the mutants. First, we performed clonogenic survival analysis (Figure 3A) in SUM149PT^{BRCA1mut} and SUM149PT^{BRCA1mut}/SHLD2 KO cell lines following exposure to PARPi (olaparib) or POLQi (ART558). Loss of SHLD2 in SUM149PT conferred resistance to olaparib (Figure 3B) but resulted in sensitization to ART558 (Figure 3C).¹³ We also observed stronger killing of SUM149PT^{BRCA1mut} and SUM149PT^{BRCA1mut}/SHLD2 cells when olaparib and ART558 were combined (Figures S2E and S2F), which is in line with our genetic POLQ KO models. Next, we performed DNA fiber analysis combined with S1 nuclease treatment (Figure 3D). In line with previous reports, we observed increased fork speed (Figure 3E) and S1 sensitivity (Figure 3F) in SUM149PT^{BRCA1mut} following olaparib exposure, indicating the formation of post-

replicative ssDNA gaps. Both fork speed and S1 sensitivity were rescued in olaparib-treated SUM149PT^{BRCA1mut}/SHLD2 KO cells (Figures 3E and 3F). Strikingly, ssDNA gap accumulation could be observed in ART558-treated SUM149PT^{BRCA1mut} cells with more pronounced effect in SUM149PT^{BRCA1mut}/SHLD2 KO cells, accompanied by only a modest fork speed increase in SUM149PT^{BRCA1mut}/SHLD2 KO (Figures 3E and 3F). These results are in line with our fork velocity data in BRCA2-depleted POLQ KO eHAP cells (Figures 1I and 2E). We also monitored fork asymmetry on exposure to olaparib or ART558 and observed results that generally correlated with ssDNA gap accumulation in these conditions (Figures S2G and S2H) and our fork asymmetry data in eHAP cells (Figure 1J). Taken together, these data indicate that defects in post-replicative ssDNA gap sealing correlate with sensitivities to PARPi or POLQi in a clinically relevant BRCA1-hypomorphic cancer models.

Biochemical reconstitution reveals the mechanisms of POLQ-mediated ssDNA gap sealing

Our results suggested a potential role for POLQ in sealing post-replicative ssDNA gaps in PARPi-treated and/or BRCA-deficient cells. To investigate if POLQ can perform such a function at the biochemical level, we designed an oligonucleotide substrate mimicking a post-replicative ssDNA gap of physiological length^{31,38} (Figure 4D, top). On addition of purified POLQ PD (Figure 4A), we observed robust 3' end extension, ssDNA gap fill-in, and 5' strand displacement (Figures 4B, S3A, and S3B), which are both fully inhibited on the addition of recombinant RPA-RFP-His₆ (referred to as RPA for brevity) (Figures 4B and 4C). Previous reports suggested that RPA does not impede primer extension by POLQ PD.⁸ However, this was likely due to the usage of 23 nt-long ssDNA overhangs—shorter than the minimal RPA binding site (30–40 nt). The inhibition of POLQ PD gap fill-in synthesis and strand displacement by RPA is alleviated by increasing concentrations of POLQ HD, indicating that POLQ HD can displace RPA to allow gap filling by POLQ PD (Figures 4D and 4E). We note that even at high concentrations, POLQ HD alone does not displace the Cy5-labeled strand. Strand displacement is observed only when POLQ PD is present, which implies the polymerase activity is the engine driving DNA strand

Figure 2. Combined POLQ loss and PARP inhibition exacerbates ssDNA gap accumulation in BRCA2-depleted cells

- (A) CellTiter-Glo analysis of cell survival of olaparib-treated POLQ +/+ and POLQ –/– eHAP cells transfected with the indicated siRNAs. All data points represent mean survival normalized to non-treated POLQ +/+ eHAP cells transfected with non-targeting siRNA. Error bars indicate SEM. Lines represent sigmoidal fits (n = 3–4).
- (B) Representative results of a single biological replicate of native CldU (ssDNA), PCNA, and DAPI staining of POLQ +/+ and POLQ –/– eHAP cells transfected with indicated siRNAs treated with indicated dose of olaparib. Red line represents cutoff for calculation of ssDNA-positive fraction of cells indicated in the upper right corner.
- (C) Quantification of global ssDNA intensity in total cell population. Boxplot graph displays median values with 10–90 percentile (N = 714–1,116 nuclei for each condition; n = 3 independent experiments). p values by Mann-Whitney test. The data presented correspond to the same dataset as data in Figure 1E.
- (D) Top: schematic illustrating DNA fiber assay protocol for POLQ +/+ and POLQ –/– (clone 4, C4) eHAP cells transfected with the indicated siRNAs treated with indicated dose of olaparib for indicated amount of time. Bottom: representative immunofluorescence images. Scale bars, 10 μ m.
- (E) Measured fork rates in POLQ +/+ and POLQ –/– (clone 4, C4) eHAP cells transfected with the indicated siRNAs treated with indicated dose of olaparib (N = 210–335 fibers for each condition, n = 2 replicates). Red lines represent mean. p values by Mann-Whitney test.
- (F) Measured length of individual dual-labeled DNA fibers in POLQ +/+ and POLQ –/– (clone 4, C4) eHAP cells transfected with the indicated siRNAs treated with indicated dose of olaparib with or without S1 nuclease treatment. Red line represents mean (N = 208–343 fibers for each condition, n = 2 replicates). p values by Mann-Whitney test.
- (A–F) n.s. p > 0.05; * p ≤ 0.05; ** p ≤ 0.01; *** p ≤ 0.001; **** p ≤ 0.0001.

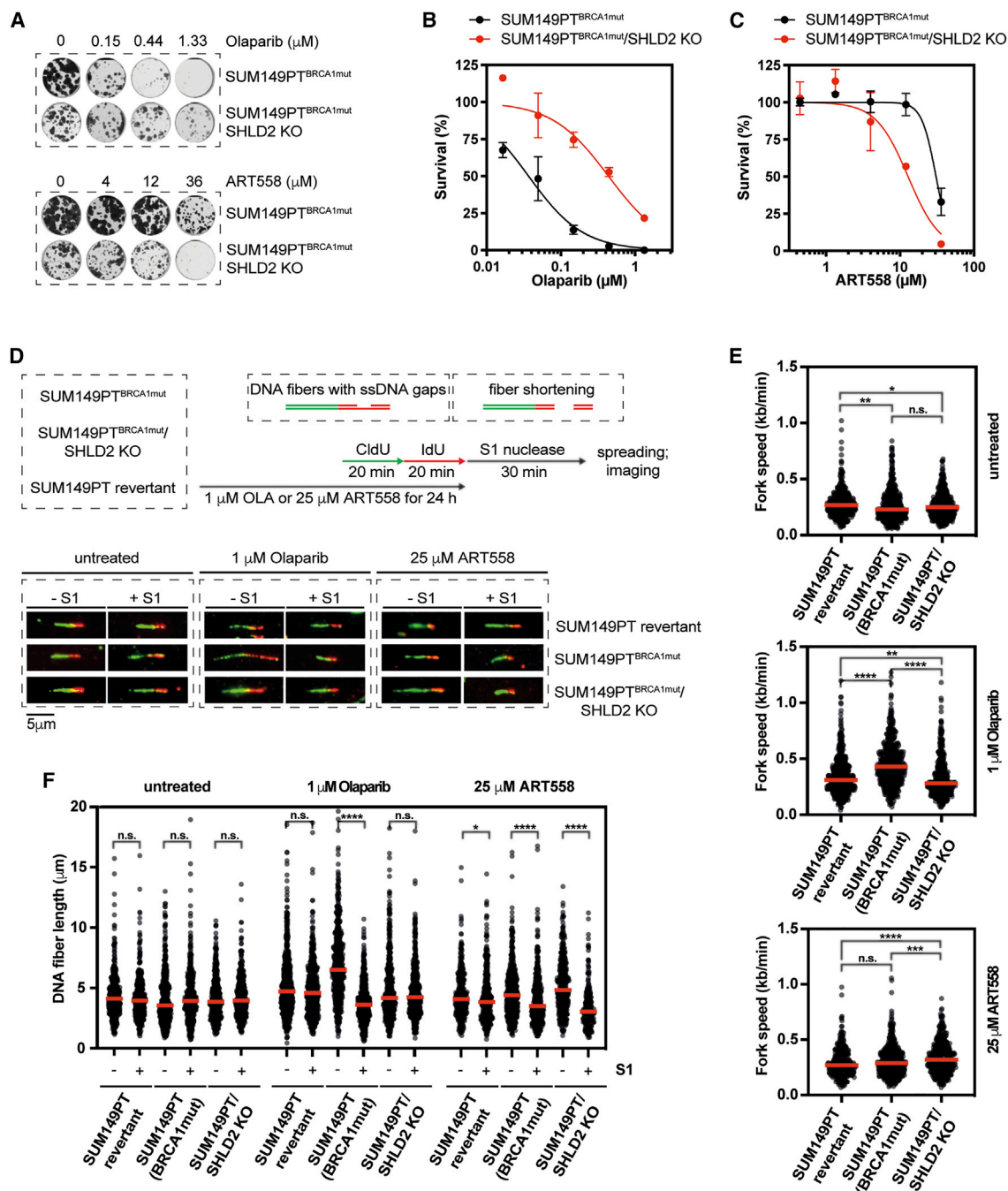


Figure 3. POLQ expose ssDNA gaps in PARPi-resistant SHLD2-deficient BRCA1 hypomorphs

(A) Representative images ($n = 3$ independent experiments) of clonogenic survival assays in SUM149PT^{BRCA1mut} and SUM149PT^{BRCA1mut}/SHLD2 KO cells treated olaparib or ART558.

(B) Quantification of clonogenic survival assays in SUM149PT^{BRCA1mut} and SUM149PT^{BRCA1mut}/SHLD2 KO cells treated with olaparib. Data represent mean \pm SEM normalized to non-treated SUM149PT^{BRCA1mut} and SUM149PT^{BRCA1mut}/SHLD2 KO cells ($n = 3$ independent experiments). Lines represent sigmoid fits.

(C) Quantification of clonogenic survival assays in SUM149PT^{BRCA1mut} and SUM149PT^{BRCA1mut}/SHLD2 KO cells treated with ART558. Data represent mean \pm SEM normalized to non-treated SUM149PT^{BRCA1mut} and SUM149PT^{BRCA1mut}/SHLD2 KO cells ($n = 3$ independent experiments). Lines represent sigmoid fits.

(legend continued on next page)

unzipping in the system. Omission of dNTPs (Figure S3C) or addition of ATP- γ -S (poorly hydrolysable ATP analog) (Figure S3D) strongly impaired the gap-filling activity of POLQ, indicating that both DNA polymerase activity of POLQ PD and ATPase activity of POLQ HD are critical. Addition of ART558 prevented primer extension by POLQ and resulted in a ladder of short extension products (Figure S3E). Using fluorescently labeled POLQ PD (Figures S4A–S4C), referred to as POLQ PD(A647), we then performed DNA capture assay using biotinylated gapped DNA substrate in the presence of ART558 and observed a significant depletion of POLQ PD(A647) from the gapped DNA substrate (Figure S4D), which confirms that ART558 inhibits primer extension by destabilizing POLQ PD-DNA complex resulting in lower processivity.

The strand displacement activity of POLQ PD could give rise to DNA flap structures in cells. Recent work exploiting whole-genome CRISPR screens revealed FEN1 as a synthetic lethal gene with loss of BRCA2⁹ with FEN1 inhibitors specifically killing BRCA-deficient cells.³⁹ During DNA replication, FEN1 cleaves flaps formed during Okazaki fragment maturation. DNA ligase 1 (LIG1) seals the resulting nicks.⁴⁰ To test whether FEN1-LIG1 can process POLQ-generated DNA flaps, we performed the reaction essentially as described in Figure 4D with the addition of purified FEN1 and LIG1 (Figures 4F and 4G). Only when FEN1 and LIG1 are both added to the reaction, we observed a sealed product formation (Figure 4H). This indicates that POLQ PD, POLQ HD, FEN1, and LIG1 are all required to seal the model RPA-coated ssDNA gap in a minimal reconstituted system.

To directly estimate the efficiency of DNA extension by POLQ PD, we employed a combination of optical tweezers, microfluidics, and fluorescence microscopy (C-TRAP, Lumicks). We used a previously established method to generate an ~ 5.4 knt-long asymmetrically positioned ssDNA gap within a 48.5 kb-long doubly biotinylated λ DNA⁴¹ tethered between two streptavidin-coated polystyrene microspheres held at 10 pN force. Double-stranded DNA (dsDNA) was stained with Sytox Orange fluorescent dye (Figure 5A). The gap-filling reaction was started by moving the DNA substrate to a microfluidic channel containing POLQ PD. A large excess of unlabeled POLQ PD was employed to minimize possible underestimation of DNA synthesis rate due to dissociation of the POLQ PD during the reaction. DNA synthesis can be then calculated directly from the slope of Sytox Orange signal in kymographs, which extends from the 3' end of the gap as dsDNA is produced (Figure 5B). Using this method, we measured the DNA extension rate of POLQ to be ~ 30 nt/min (Figure 5C), which is relatively fast considering we 300–500 nt/min fork rates in DNA fiber experiments allowing POLQ to reach the end of 70 nt-long gap in ~ 2 min. Importantly, DNA extension was inhibited by POLQ inhibitor or addition of RPA-

EGFP confirming our ensemble data (Figures 5B and 5C). Next, we measured the rate of RPA-EGFP displacement by POLQ HD (Figure 5D), which was very rapid with an estimated 400 nt/min clearance rate (Figures 5E and 5F), similar to previously reported values.⁴² This indicates that DNA synthesis by POLQ PD is the rate limiting step of the reaction. The RPA stripping by POLQ HD is completely inhibited in the presence of ATP- γ -S (Figures 5G and 5H) validating our previous bulk data (Figure S3D).

POLQ can utilize microhomology during ssDNA gap sealing

Microhomology-flanking small deletions are an established hallmark of POLQ activity in HR-deficient cells.² Genomic approaches in *C. elegans* demonstrated the formation of POLQ-mediated deletions with a minimum of 1 nt microhomology in response to treatment with replication-blocking agents⁶ and at sites of hard-to-replicate G4-DNA structures,⁴³ which were proposed to arise by MMEJ repair of resected DSBs or broken RFs. To reconcile these data with POLQ-mediated gap sealing, we envisioned two possibilities.

First, POLQ may act as a translesion polymerase to bypass endogenous lesions skipped over by the replisome.⁴⁰ This is supported by POLQ PD inserting nucleotides opposite tetrahydrofuran and thymidine glycol *in vitro*⁴⁴ and global reduction in specific single-nucleotide substitutions in *polq-1* animals.⁴⁵ To test whether POLQ can carry out translesion DNA synthesis (TLS) in cells, we performed DNA fiber analysis of eHAP WT and POLQ KO cells irradiated with ultraviolet C light (UVC) (Figure S5A) and analyzed RF progression. We observed a significant fork slowing in POLQ KO cells on UVC exposure (Figures S5B and S5C) and increased fork asymmetry (Figure S5D), which is consistent with reported impaired fork progression following UVC treatment in POLQ-deficient MEFs⁴⁶ and recruitment of POLQ PD to chromatin following UVC irradiation in human cells.⁴ Recently, a synthetic lethality between Pol zeta and BRCA-deficiency accompanied by post-replicative ssDNA gap accumulation was reported.⁴⁷ Therefore, we treated POLQ KO cells with Pol zeta inhibitor, JH-RE-06. POLQ KO cells were sensitive to JH-RE-06 irrespective of the BRCA2 status (Figure S5E), indicating that POLQ and Pol zeta act in parallel pathways in BRCA2-proficient and deficient cells. However, combination of JH-RE-06 and ART558 did not induce synergistic cell killing (Figure S5F).

POLQ-mediated TLS does not explain the major POLQ-dependent signature of in HR-deficient cells—microhomology-containing deletions. We reasoned that these signatures could also arise during post-replicative ssDNA gap filling by POLQ without the need for a DNA break with POLQ utilizing

(D) Top: schematic illustrating DNA fiber assay protocol for analysis of fork dynamics in indicated cell lines treated with indicated dose of olaparib or ART558 for 24 h with or without S1 nuclease treatment. Bottom: representative immunofluorescence images of the experiment.

(E) Measured fork rates in SUM149PT revertant, SUM149PT^{BRCA1mut}, and SUM149PT^{BRCA1mut}/SHLD2 KO cells treated with olaparib or ART558 (N = 312–585 fibers for each condition, n = 2–3 independent experiments). Red line represents median. p values by Mann-Whitney test.

(F) Measured length of individual dual-labeled DNA fibers in SUM149PT revertant, SUM149PT^{BRCA1mut}, and SUM149PT^{BRCA1mut}/SHLD2 KO cells treated with olaparib or ART558 with or without S1 nuclease treatment. Red line represents median (N = 270–585 fibers for each condition, n = 2–3 independent experiments). p values by Mann-Whitney test.

(A–F) n.s. p > 0.05; * p ≤ 0.05; ** p ≤ 0.01; *** p ≤ 0.001; **** p ≤ 0.0001.

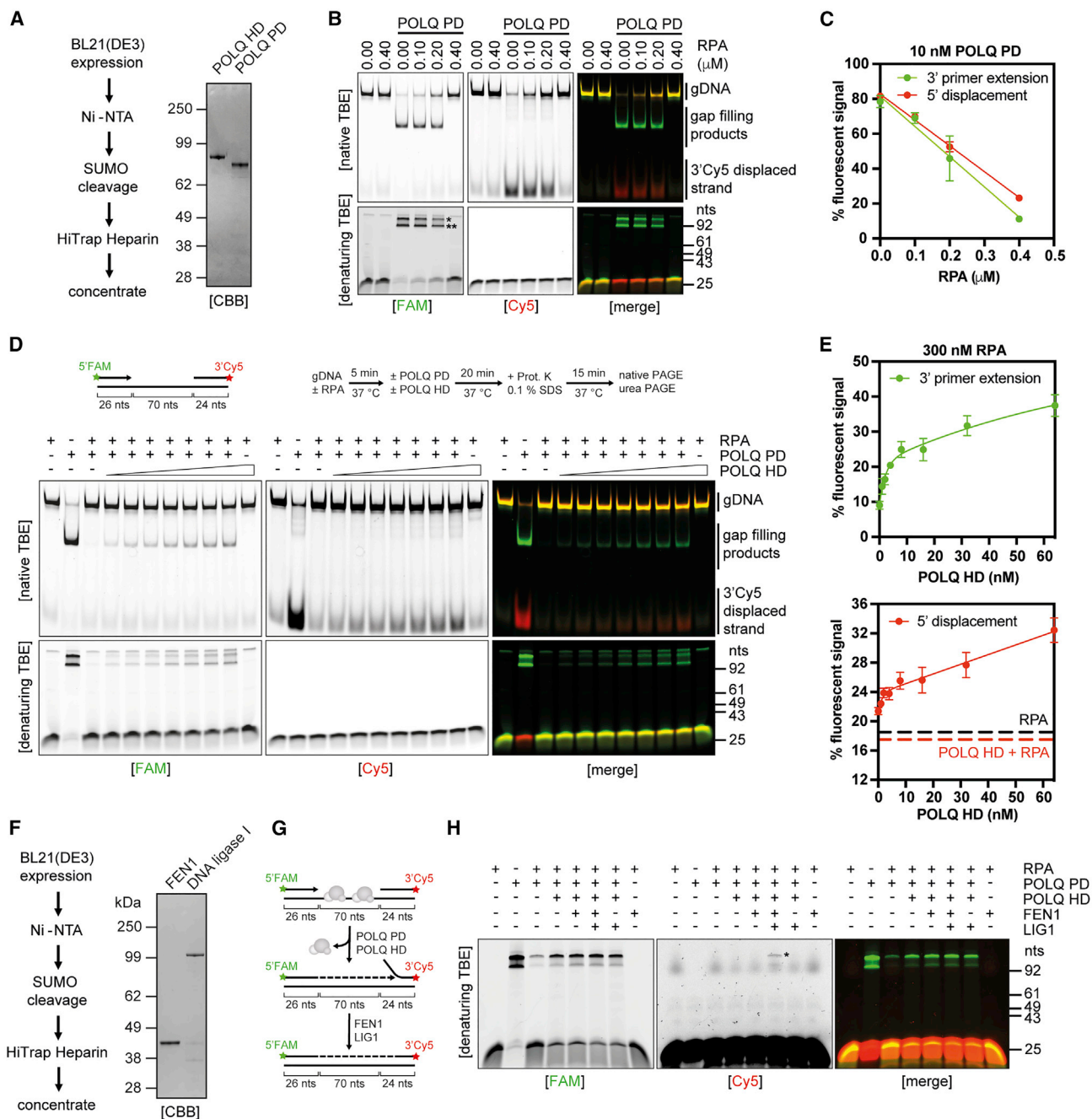


Figure 4. Reconstitution of POLQ-dependent sealing of post-replicative gaps *in vitro*

(A) Schematic of expression and purification protocol for POLQ PD and HD. Coomassie brilliant blue staining of SDS-PAGE resolved POLQ PD and POLQ HD. 0.5 μg of purified protein was loaded.

(B) Gapped DNA substrate was pre-incubated with indicated RPA concentrations. Reaction was performed and analysis on native PAGE or denaturing urea PAGE as in (D).

(C) Percentage of FAM-labeled oligonucleotide extension product formation and percentage of Cy5-labeled DNA strand displacement as a function of RPA concentration. Data points indicate mean ± SEM. Lines represent linear fits (n = 3 independent experiments).

(D) Top right: schematic of oligonucleotide-based post-replicative ssDNA gap substrate. Top left: schematic of gap-filling reaction reconstituted *in vitro*. Bottom: representative native or denaturing PAGE gels of indicated reactions. POLQ HD was added in increasing concentrations together with 10 nM POLQ PD to RPA-bound gapped DNA substrate. Single asterisk (*) denotes full-length (120 nt) extension product. Double asterisk (**) denotes an approach product terminating before 5' ds-ssDNA junction (~96 nt).

(legend continued on next page)

microhomology within the ssDNA gap. We termed this hypothetical activity as MMGS. To test whether MMGS can occur, we engineered a series of substrates containing a ssDNA tail increasing microhomology size complementary to a sequence within the ssDNA gap 35 nucleotides upstream of the original 3' ss-dsDNA junction (Figure 6A). MMGS coupled with strand displacement would generate 85 nt-long deletion products. Addition of a single nucleotide mismatched tail reduced the gap-filling efficiency to ~10% compared with the unaltered DNA substrate. Increasing the length of microhomology from 1 to 5 nt restored the overall DNA extension efficiency to ~40%, with a noticeable DNA extension efficiency increase starting at 4 nt microhomology length (Figures 6B–6F) consistent with 4 nt microhomology requirement for efficient MMEJ with model DSB substrates *in vitro*.⁴⁸ Notably, ~85 nt-long MMGS product appears, when 4 nt-long microhomology substrate is used, and becomes the major product with 5 nt-long microhomology (Figure 6B). Minor shorter product likely results from a second upstream microhomology utilization by MMGS. Klenow fragment of *E. coli* DNA polymerase I with high structural similarity to POLQ PD⁴⁹ supports DNA synthesis through the unaltered gapped DNA substrate yielding a major ~120 nt-long product. No DNA synthesis was observed, when 5 nt-long microhomology tail was added (Figure 6G) confirming that MMGS is POLQ-specific. POLQ PD-mediated strand displacement reaction follows a similar pattern to DNA extension (Figures 6E, 6F, and S5G); however, at 5 nt-long microhomology, a decrease in the efficiency can be observed (Figure 6F). We reasoned that in addition to expected reaction in *cis*, small portion of reaction can occur in *trans* with longer (5 nt) microhomologies (Figure 6H). To address this, we performed MMGS using 5 nt-long microhomology substrate performed in the presence of unlabeled bottom strand competitor (Figure 6H). We were able to observe a small fraction of DNA synthesis taking place in *trans* (Figures 6I and 6J) explaining the reduction of Cy5-labeled displacement product (Figures 6F and S5G).

Taken together, we demonstrate that POLQ PD can catalyze a unique mutagenic gap-filling reaction referred to as MMGS, which through annealing of microhomologies results in deletion formation during the gap-filling reaction. We propose that MMGS catalyzed by POLQ during post-replicative ssDNA gap filling could contribute to the frequent POLQ-dependent genomic scars found in HR-deficient cancers *in vivo* (Figure 7).

DISCUSSION

POLQ was identified over a decade ago as a key effector of DSB repair by MMEJ.⁵⁰ It was assumed that the major role

of POLQ is in MMEJ, which is supported by ionizing radiation (IR) sensitivity of POLQ-deficient MEFs¹³ and nematode strains.⁵¹ Furthermore, synthetic lethality between POLQ loss and HR-deficiency as well as POLQ-dependent microhomology-containing deletions were proposed to arise by the POLQ-mediated MMEJ reaction.^{4,7} However, recent unbiased high-throughput approaches provide further insight into POLQ biology, which suggest a broader role of this protein distinct from DSB repair. In a recent whole-genome CRISPR and shRNA screening in a BRCA2 hypomorphic colon cancer cell line,⁹ POLQ dropped out as a major hit together with multiple members of the lagging strand processing and base-excision repair machineries such as FEN1, APEX2, LIG1, and XRCC1. Furthermore, a CRISPRi-based repair screen using a targeted DNA damage response library⁵² recently demonstrated that POLQ generates targeted genomic DNA repair outcomes that cluster with replication checkpoint genes (RAD17, RAD9A, HUS1, and RAD1). Finally, proteomic profiling of UV-treated sperm chromatin in *Xenopus* egg extract identified POLQ among proteins enriched on chromatin on UV damage together with many other replication-stress response and TLS factors.⁵³

In this study, we now show that POLQ prevents the accumulation of ssDNA and post-replicative ssDNA gaps in BRCA1 hypomorphs and BRCA2-depleted cells. We further show that the increase in ssDNA levels is exacerbated by deletion of BRCA2 or PARPi treatment. We propose that the accumulation of ssDNA gaps in POLQ-deficient cells and exacerbation by PARPi treatment likely explains the observed POLQ-PARPi synergy in killing of BRCA-deficient cancer cells.^{5,13} The synergy of POLQ-PARPi is currently being explored in ongoing phase I/IIa clinical trials with a combination of ART4215 and Talazoparib in patients with cancers that harbor defects in DNA repair.⁵⁴ It has to be noted, however, that we detect high levels of ssDNA gaps in G2 cells in BRCA2-depleted POLQ KOs in addition to ssDNA accumulating in S-phase cells. These findings are consistent with recently published work implicating POLQ in the repair of DSBs via MMEJ in G2/M.^{55,56} It seems plausible that both ssDNA gap sealing and MMEJ activities of POLQ are important for survival of BRCA-deficient cells in a specific context. POLQ may seal ssDNA gaps in late S or G2/M, but if ssDNA gaps are ultimately converted to DSBs during late G2/M, POLQ can repair these breaks via MMEJ.

Given PARP inhibition is proposed to cause skipping of various lesions by the replisome,^{22,30} it is likely that the role of POLQ in post-replicative gap filling is to carry out DNA synthesis across a range of lesion types. Previous work in *C. elegans*⁵⁷ and mice,⁴⁶ together with our data, indicates

(E) Top: percentage of FAM-labeled oligonucleotide extension product as a function of POLQ HD concentration. Data points indicate mean \pm SEM. Line represents double-exponential fit ($n = 3$ independent experiments). Bottom: percentage of displaced Cy5-labeled DNA strand as a function of POLQ HD. Dotted lines represent mean values of controls lacking POLQ PD. Data points indicate mean \pm SEM. Full lines represent double-exponential fit ($n = 3$ independent experiments).

(F) Schematic of expression and purification protocol for FEN1 and LIG1. Coomassie brilliant blue staining of SDS-PAGE resolved FEN1 and LIG1. 0.5 μ g of purified protein was loaded.

(G) Schematic of expected full gap sealing reaction yielding dual-labeled (FAM-Cy5) DNA product.

(H) RPA-bound gapped substrate was incubated in the presence of indicated proteins and resolved by denaturing urea-PAGE to monitor FAM-labeled strand extension and ligation with Cy5-labeled second strand. Ligation product of the full reaction is indicated by asterisk (*).

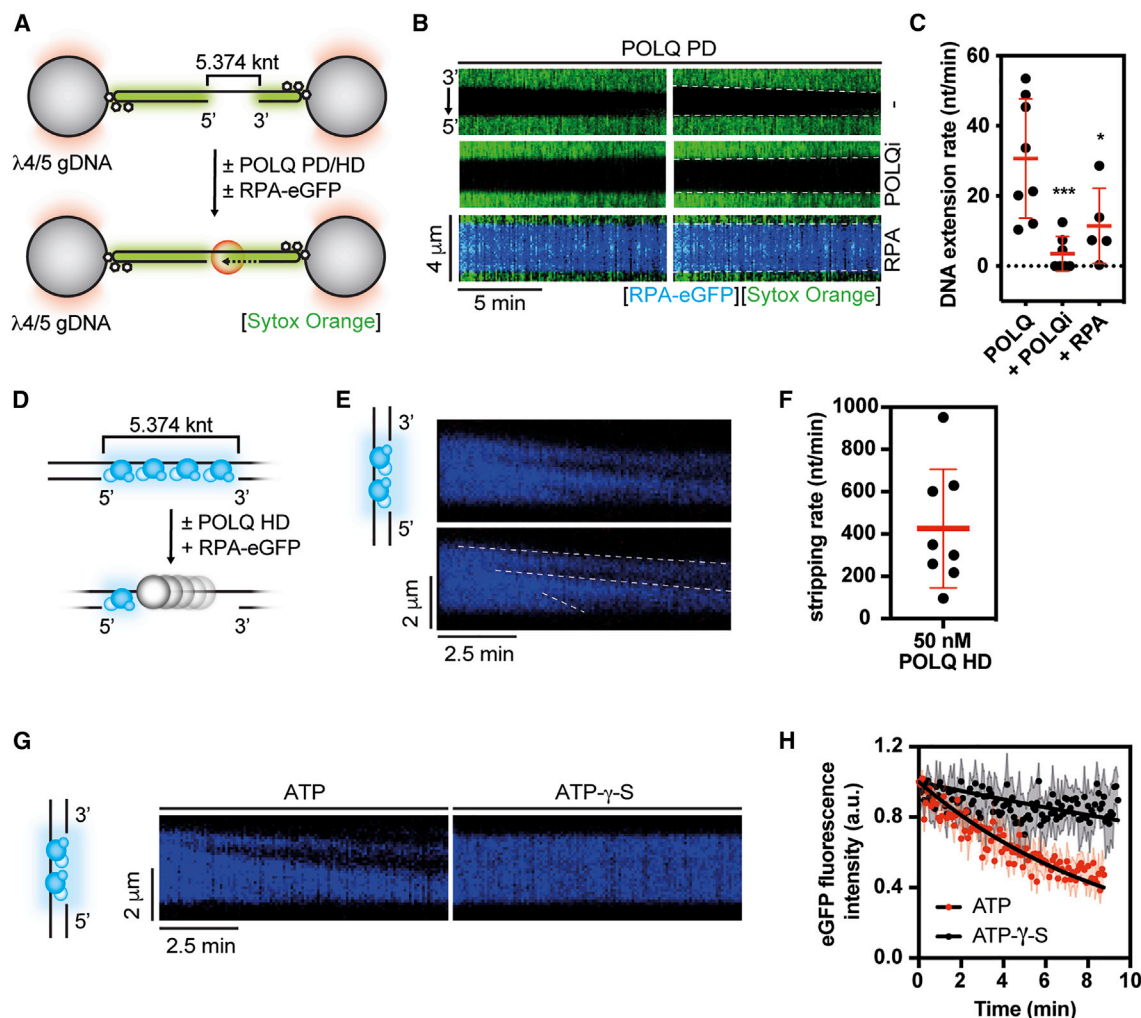
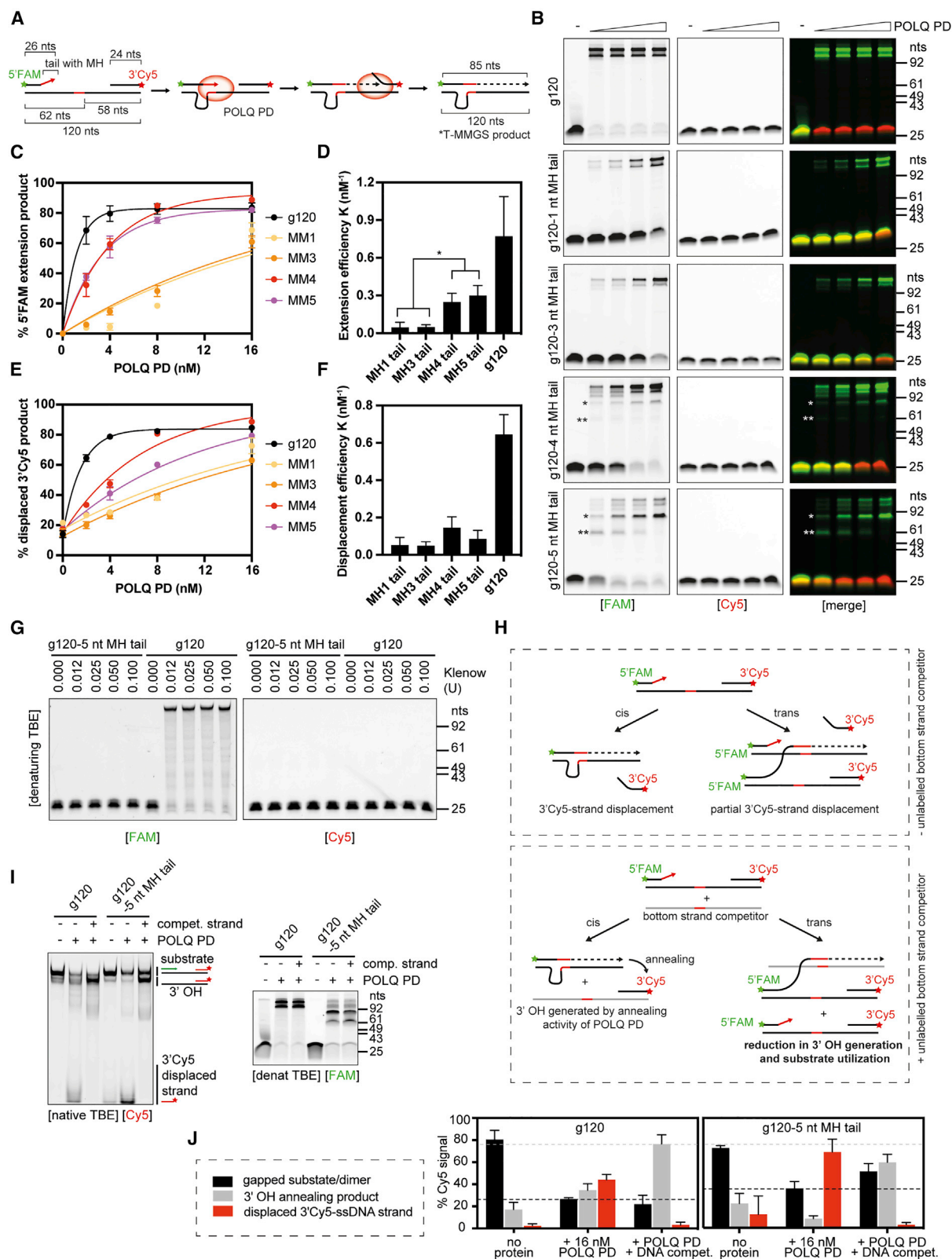


Figure 5. Single-molecule imaging of POLQ-mediated ssDNA gap sealing

(A) Schematics of the experimental set-up of the optical tweezer (C-Trap) system to observe 3' DNA end extension.
 (B) Representative kymographs showing the extension of 3' DNA end at the edge of the ssDNA gap by POLQ PD. DNA stained by Sytox Orange (green) in the presence or absence of 1 nM RPA-EGFP or 10 μ M POLQ inhibitor (ART558). When present, RPA-EGFP signal is shown in blue. DNA extension rate was measured as a slope of the border of spreading Sytox Orange signal.
 (C) Quantification of DNA extension rates in indicated conditions. Each dot represents a single gapped λ DNA molecule. Red lines represent mean \pm SD.
 (D) Schematics of the experimental set-up of the optical tweezer (C-Trap) system to observe RPA-EGFP stripping from gapped λ DNA molecules. 5 nM RPA-EGFP was pre-bound to gapped λ DNA molecules before incubation in channel containing 50 nM POLQ HD.
 (E) Representative kymograph showing unidirectional RPA-EGFP displacement by POLQ HD in the presence of ATP. RPA-EGFP signal is shown in blue. RPA-stripping rate was measured as a slope of the border of loss of RPA-EGFP signal.
 (F) Quantification of RPA-stripping rates in indicated conditions. Each dot represents a single stripping event. Stripping rate in nm/min was converted to nt/min based on known ssDNA gap length. Red lines represent mean \pm SD.
 (G) Representative kymographs of stripping of RPA-EGFP by POLQ HD in the presence of ATP or ATP- γ -S.
 (H) Removal of RPA-EGFP from gapped ssDNA measured as relative EGFP fluorescence intensity as a function of time in indicated conditions (N = 5 molecules per condition). Shaded area represents SEM. Black lines represent exponential fits.

that indeed POLQ is capable of TLS across UVC-generated lesions. However, the nature of the endogenous lesion that is bypassed by POLQ-mediated MMS remains unclear. Among the candidates are base excision repair (BER) intermediates resulting from misincorporated cytotoxic nucleotides.^{30,58} Another possibility constitute toxic DNA adducts resulting from metabolism of endogenous aldehydes.⁵⁹ These lesions

are processed by the Fanconi anemia pathway, which repairs DNA inter-strand crosslinks. Consistently, POLQ loss has been shown to be synthetically lethal with loss of FANCD2 in mice.⁴ Similarly, *polq-1* mutant nematodes are sensitive to DNA inter-strand crosslinking agents,⁵¹ with *polq-1* and other Fanconi genes such as *dog-1* and *helq-1* acting in parallel pathways.^{43,51}



(legend on next page)

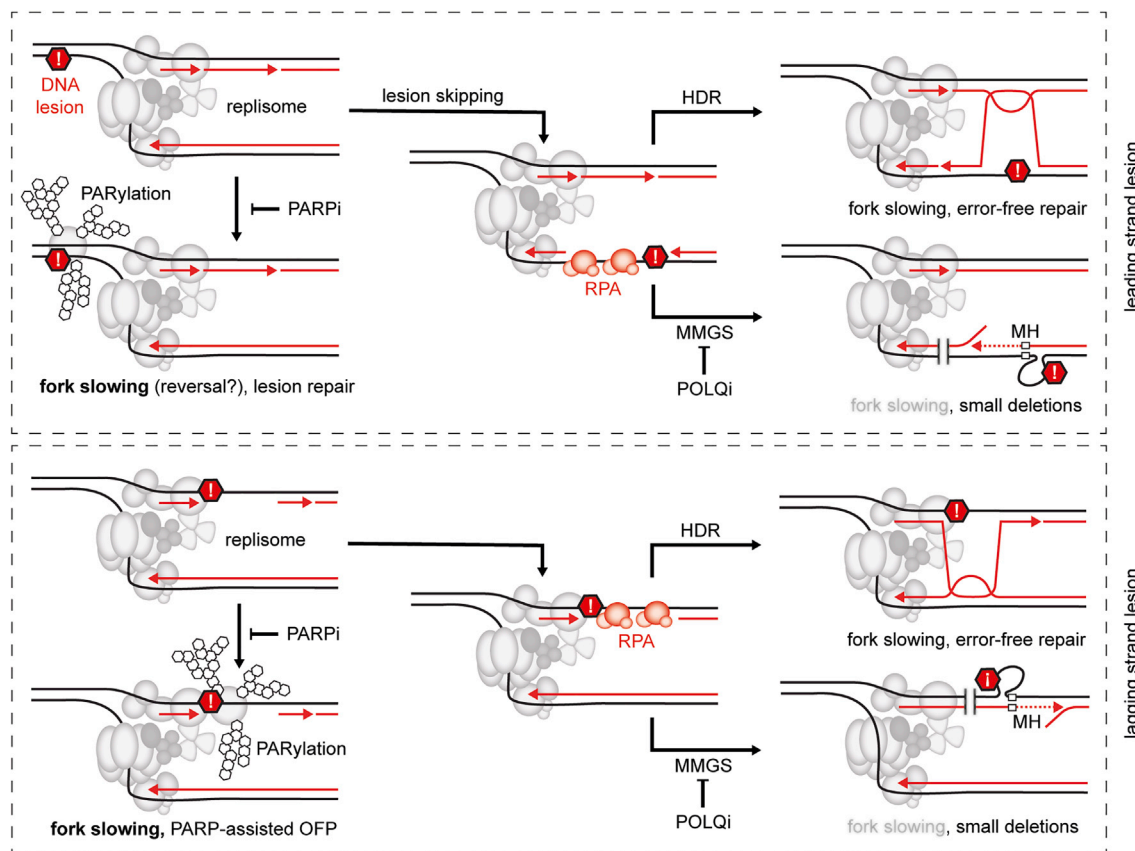


Figure 7. Potential role of POLQ, HR, and PARYlation in post-replicative ssDNA gap sealing and genome stability maintenance

Model depicting the function of POLQ and HR in sealing RPA-coated ssDNA gaps forming behind the replisome as a result of potential leading strand lesion skipping and/or defective lagging strand processing exacerbated by PARPi. HDR, homology-directed repair.

The MMGS mechanisms proposed here would also allow for efficient lesion bypass and through its propensity to create microhomology-containing deletions and could give rise to the mutation signature of POLQ activity in HR-deficient cells *in vivo*. We also note that from genomic studies in

C. elegans, the average length of POLQ-mediated deletions is ~20 bp,² which is very well consistent with average length of post-replicative ssDNA gaps.³¹ Intriguingly, MMGS would allow for the bypass of a variety of lesions since it does not require nucleotide incorporation opposite the lesion like

Figure 6. Microhomology-mediated gap skipping (MMGS) as a potential mechanism generating POLQ-dependent genomic scars

- (A) Schematic of oligonucleotide-based MMGS substrate. The expected reaction process and product is indicated.
- (B) Representative denaturing PAGE gels of MMGS reactions with substrates with microhomology-containing 3' ssDNA tail of indicated length. Primary (*) and secondary (**) microhomology-containing deletion products are indicated by asterisks.
- (C) Percentage of FAM (fluorescein)-labeled oligonucleotide extension product as a function of POLQ PD concentration for individual MMGS substrates. Data points indicate mean \pm SEM. Lines represent single-exponential fits ($n = 3-4$ independent experiments).
- (D) DNA extension efficiency calculated from fits in (C). Error bars represent error of the fit. p values by one-way ANOVA, n.s. $p > 0.05$; * $p \leq 0.05$; ** $p \leq 0.01$; *** $p \leq 0.001$; **** $p \leq 0.0001$.
- (E) Percentage of Cy5-labeled strand displacement product as a function of POLQ PD concentration for individual MMGS substrates. Data points indicate mean \pm SEM. Lines represent single-exponential fits ($n = 3-4$ independent experiments).
- (F) DNA strand displacement efficiency calculated from fits in Figure 5E for the indicated MMGS substrates. Error bars represent error of the fit.
- (G) Representative denaturing PAGE gels of MMGS reactions with indicated substrates in the presence of Klenow fragment.
- (H) Schematic of possible reaction outcomes with longer microhomologies. 30 nM unlabeled bottom strand added to distinguish *cis* and *trans* contribution. OH, overhang.
- (I) Left: representative native PAGE gel of reactions with indicated substrates. Right: representative denaturing PAGE gel of MMGS reactions with indicated substrates.
- (J) Quantification of reaction shown in (I) ($n = 3$ independent experiments, error bars represent SD). Decreased substrate utilization and 3'OH production indicate a portion of reaction is occurring in *trans*.

abnormally stable DNA secondary structure, which in principle would not be possible to bypass by canonical TLS but would be potentially skippable by MMS. Endogenous G4s were shown to be a target of POLQ-mediated scarring in *C. elegans*.⁴³ G4-stabilizing ligands also restore PARPi sensitivity in cells dually deficient in BRCA1 and 53BP1⁶⁰ similarly to POLQ.¹³ Finally, G4s have an increased propensity to form on lagging strand during DNA replication.⁶¹ Given the aforementioned genetic clustering of POLQ with enzymes such as FEN1 and LIG1,⁹ the ability of FEN1-LIG1 to seal ssDNA gaps in our reconstituted system, and the general phenomenon of PARPi sensitization and BRCA-deficient cancer cell killing by perturbation of lagging strand processing, it is tempting to speculate that POLQ may seal ssDNA gaps on the lagging strand (Figure 7).

In summary, the work presented here reveals an unappreciated role for POLQ in post-replicative ssDNA gap filling and provides insight into the mechanisms underlying the use of POLQ inhibitors in BRCA-deficient cancers.

Limitations of the study

The work is mostly limited to specific *ex vivo* systems, eHAP and SUM149PT cell lines. Our results agree well with values we have reported previously for eHAP cell lines with or without BRCA2 depletion³⁰; however, studies with different human cell lines reported pronounced RF slowing in HR-deficient cells.^{23,62} This needs to be taken into consideration when comparing reported data. Given the reductionist approach, other components of the *in vitro* gap sealing reactions are not present. It also remains to be determined how full-length human POLQ may influence MMS and RPA stripping.

STAR★METHODS

Detailed methods are provided in the online version of this paper and include the following:

- KEY RESOURCES TABLE
- RESOURCE AVAILABILITY
 - Lead contact
 - Materials availability
 - Data and code availability
- EXPERIMENTAL MODEL AND SUBJECT DETAILS
 - Bacterial strains
 - Cell lines
- METHOD DETAILS
 - Generation of CRISPR knockout cell lines
 - RNA interference
 - Drug treatment and cell survival analysis using colony formation assay and CellTiter-Glo assay
 - Western blotting
 - Indirect immunofluorescence
 - Extrachromosomal luminescence-based MMEJ assay
 - DNA fiber analysis with S1 nuclease digestion
 - Protein expression and purification
 - Expression and purification of fluorescently labelled POLQ PD variants
 - Oligonucleotide substrate preparation

- DNA extension assay
- Gap sealing assay
- DNA capture assay
- Substrate preparation for single-molecule analysis
- DNA micromanipulation, optical trapping, and fluorescence imaging

● QUANTIFICATION AND STATISTICAL ANALYSIS

SUPPLEMENTAL INFORMATION

Supplemental information can be found online at <https://doi.org/10.1016/j.molcel.2022.11.008>.

ACKNOWLEDGMENTS

Work in the Boulton lab is supported by the Francis Crick Institute (cc2098), European Research Council Advanced Investigator (TelMetab), Wellcome Trust Senior Investigator grants, and CRUK RadNet City of London. The Single Molecule Imaging Group is funded by a core grant of the MRC-London Institute of Medical Sciences (UKRI MC-A658-5TY10). S.J.B. and D.S.R. are also funded by a Wellcome Trust Collaborative Grant (P67153). Work in the West group is supported by the Francis Crick Institute (cc2098), BBSRC (BB/W01355X/1), and the Louis-Jeantet Foundation. Work in the Higgins lab is funded by the CRUK RadNet Oxford and CRUK Clinician Scientist funding (C34326/A19590). S.S.-B. was the recipient of an EMBO LT Fellowship (ALTF 707-2019) and an MSCA-IF (886577).

AUTHOR CONTRIBUTIONS

S.J.B. and O.B. conceived the study. A.V. made comments. O.B. and R.A. expressed, purified, and fluorescently labeled the proteins and performed single-molecule and ensemble assays; O.B., M.S., M.A., and A.V. performed a subset of cell-based assays and analyzed the data. V.G., J.N., G.S.H., and G.C.M.S. generated SUM149PT-derived cell lines and performed a subset of assays. S.S.-B. and G.H. generated POLQ KO cells. O.B. and S.J.B. wrote the manuscript with editorial help from R.A., M.A., M.S., R.B., and D.S.R.

DECLARATION OF INTERESTS

S.J.B. is a co-founder, VP Science Strategy and a shareholder of Artios Pharma Ltd. G.S.H. received consultancy fees from and is a shareholder of Artios Pharma Ltd and is a member of the *Molecular Cell* advisory board. V.G., J.N., H.M.R.R., and G.C.M.S. are all employees and shareholders of Artios Pharma Ltd. G.C.M.S. is a shareholder of AstraZeneca PLC.

Received: June 6, 2022

Revised: October 19, 2022

Accepted: November 8, 2022

Published: November 30, 2022

REFERENCES

1. Chapman, J.R., Taylor, M.R., and Boulton, S.J. (2012). Playing the end game: DNA double-strand break repair pathway choice. *Mol. Cell* 47, 497–510. <https://doi.org/10.1016/j.molcel.2012.07.029>.
2. Kamp, J.A., van Schendel, R., Dilweg, I.W., and Tijsterman, M. (2020). BRCA1-associated structural variations are a consequence of polymerase theta-mediated end-joining. *Nat. Commun.* 11, 3615. <https://doi.org/10.1038/s41467-020-17455-3>.
3. Lemée, F., Bergoglio, V., Fernandez-Vidal, A., Machado-Silva, A., Pillaire, M.J., Bieth, A., Gentil, C., Baker, L., Martin, A.L., Leduc, C., et al. (2010). DNA polymerase theta up-regulation is associated with poor survival in breast cancer, perturbs DNA replication, and promotes genetic instability.

- Proc. Natl. Acad. Sci. USA 107, 13390–13395. <https://doi.org/10.1073/pnas.0910759107>.
4. Ceccaldi, R., Liu, J.C., Amunugama, R., Hajdu, I., Primack, B., Petalcorin, M.I., O'Connor, K.W., Konstantinopoulos, P.A., Elledge, S.J., Boulton, S.J., et al. (2015). Homologous-recombination-deficient tumours are dependent on Pol θ -mediated repair. *Nature* 518, 258–262. <https://doi.org/10.1038/nature14184>.
5. Zhou, J., Gelot, C., Pantelidou, C., Li, A., Yücel, H., Davis, R.E., Färkkilä, A., Kochupurakkal, B., Syed, A., Shapiro, G.I., et al. (2021). A first-in-class polymerase theta inhibitor selectively targets homologous-recombination-deficient tumors. *Nat. Cancer* 2, 598–610. <https://doi.org/10.1038/s43018-021-00203-x>.
6. van Schendel, R., van Heteren, J., Welten, R., and Tijsterman, M. (2016). Genomic scars generated by polymerase theta reveal the versatile mechanism of alternative end-joining. *PLoS Genet.* 12, e1006368. <https://doi.org/10.1371/journal.pgen.1006368>.
7. Mateos-Gomez, P.A., Gong, F., Nair, N., Miller, K.M., Lazzarini-Denchi, E., and Sfeir, A. (2015). Mammalian polymerase θ promotes alternative NHEJ and suppresses recombination. *Nature* 518, 254–257. <https://doi.org/10.1038/nature14157>.
8. Mateos-Gomez, P.A., Kent, T., Deng, S.K., McDevitt, S., Kashkina, E., Hoang, T.M., Pomerantz, R.T., and Sfeir, A. (2017). The helicase domain of Pol θ counteracts RPA to promote alt-NHEJ. *Nat. Struct. Mol. Biol.* 24, 1116–1123. <https://doi.org/10.1038/nsm.3494>.
9. Mengwasser, K.E., Adeyemi, R.O., Leng, Y., Choi, M.Y., Clairmont, C., D'Andrea, A.D., and Elledge, S.J. (2019). Genetic screens reveal FEN1 and APEX2 as BRCA2 synthetic lethal targets. *Mol. Cell* 73, 885–899.e6. <https://doi.org/10.1016/j.molcel.2018.12.008>.
10. Liang, L., Deng, L., Nguyen, S.C., Zhao, X., Maulion, C.D., Shao, C., and Tischfield, J.A. (2008). Human DNA ligases I and III, but not ligase IV, are required for microhomology-mediated end joining of DNA double-strand breaks. *Nucleic Acids Res.* 36, 3297–3310. <https://doi.org/10.1093/nar/gkn184>.
11. Simsek, D., Brunet, E., Wong, S.Y., Katyal, S., Gao, Y., McKinnon, P.J., Lou, J., Zhang, L., Li, J., Rebar, E.J., et al. (2011). DNA ligase III promotes alternative nonhomologous end-joining during chromosomal translocation formation. *PLoS Genet.* 7, e1002080. <https://doi.org/10.1371/journal.pgen.1002080>.
12. Audebert, M., Salles, B., and Calsou, P. (2004). Involvement of poly(ADP-ribose) polymerase-1 and XRCC1/DNA ligase III in an alternative route for DNA double-strand breaks rejoining. *J. Biol. Chem.* 279, 55117–55126. <https://doi.org/10.1074/jbc.M404524200>.
13. Zatreanu, D., Robinson, H.M.R., Alkhatib, O., Boursier, M., Finch, H., Geo, L., Grande, D., Grinkevich, V., Heald, R.A., Langdon, S., et al. (2021). Pol θ inhibitors elicit BRCA-gene synthetic lethality and target PARP inhibitor resistance. *Nat. Commun.* 12, 3636. <https://doi.org/10.1038/s41467-021-23463-8>.
14. Gupta, R., Somyajit, K., Narita, T., Maskey, E., Stanlie, A., Kremer, M., Typas, D., Lammers, M., Mailand, N., Nussenzweig, A., et al. (2018). DNA repair network analysis reveals shieldin as a key regulator of NHEJ and PARP inhibitor sensitivity. *Cell* 173, 972–988.e23. <https://doi.org/10.1016/j.cell.2018.03.050>.
15. Dev, H., Chiang, T.W., Lescale, C., de Krijger, I., Martin, A.G., Pilger, D., Coates, J., Sczaniecka-Clift, M., Wei, W., Ostermaier, M., et al. (2018). Shieldin complex promotes DNA end-joining and counters homologous recombination in BRCA1-null cells. *Nat. Cell Biol.* 20, 954–965. <https://doi.org/10.1038/s41556-018-0140-1>.
16. Mirman, Z., Lottersberger, F., Takai, H., Kibe, T., Gong, Y., Takai, K., Bianchi, A., Zimmermann, M., Durocher, D., and de Lange, T. (2018). 53BP1-RIF1-shieldin counteracts DSB resection through CST- and Polalpha-dependent fill-in. *Nature* 560, 112–116. <https://doi.org/10.1038/s41586-018-0324-7>.
17. Noordermeer, S.M., Adam, S., Setiawati, D., Barazas, M., Pettitt, S.J., Ling, A.K., Olivieri, M., Álvarez-Quilón, A., Moatti, N., Zimmermann, M., et al. (2018). The shieldin complex mediates 53BP1-dependent DNA repair. *Nature* 560, 117–121. <https://doi.org/10.1038/s41586-018-0340-7>.
18. Ghezraoui, H., Oliveira, C., Becker, J.R., Bilham, K., Moralli, D., Anzilotti, C., Fischer, R., Deobagkar-Lele, M., Sanchiz-Calvo, M., Fueyo-Marcos, E., et al. (2018). 53BP1 cooperation with the REV7-shieldin complex underpins DNA structure-specific NHEJ. *Nature* 560, 122–127. <https://doi.org/10.1038/s41586-018-0362-1>.
19. Luedeman, M.E., Stroik, S., Feng, W., Luthman, A.J., Gupta, G.P., and Ramsden, D.A. (2022). Poly(ADP) ribose polymerase promotes DNA polymerase theta-mediated end joining by activation of end resection. *Nat. Commun.* 13, 4547. <https://doi.org/10.1038/s41467-022-32166-7>.
20. Ray Chaudhuri, A., Hashimoto, Y., Herrador, R., Neelsen, K.J., Fachinetti, D., Bermejo, R., Cocito, A., Costanzo, V., and Lopes, M. (2012). Topoisomerase I poisoning results in PARP-mediated replication fork reversal. *Nat. Struct. Mol. Biol.* 19, 417–423. <https://doi.org/10.1038/nsm.2258>.
21. Berti, M., Cortez, D., and Lopes, M. (2020). The plasticity of DNA replication forks in response to clinically relevant genotoxic stress. *Nat. Rev. Mol. Cell Biol.* 21, 633–651. <https://doi.org/10.1038/s41580-020-0257-5>.
22. Maya-Mendoza, A., Moudry, P., Merchut-Maya, J.M., Lee, M., Strauss, R., and Bartek, J. (2018). High speed of fork progression induces DNA replication stress and genomic instability. *Nature* 559, 279–284. <https://doi.org/10.1038/s41586-018-0261-5>.
23. Cong, K., Peng, M., Kousholt, A.N., Lee, W.T.C., Lee, S., Nayak, S., Krais, J., VanderVere-Carozza, P.S., Pawelczak, K.S., Calvo, J., et al. (2021). Replication gaps are a key determinant of PARP inhibitor synthetic lethality with BRCA deficiency. *Mol. Cell* 81, 3128–3144.e7. <https://doi.org/10.1016/j.molcel.2021.06.011>.
24. Panzarino, N.J., Krais, J.J., Cong, K., Peng, M., Mosqueda, M., Nayak, S.U., Bond, S.M., Calvo, J.A., Doshi, M.B., Bere, M., et al. (2021). Replication gaps underlie BRCA deficiency and therapy response. *Cancer Res.* 81, 1388–1397. <https://doi.org/10.1158/0008-5472.CAN-20-1602>.
25. Fernandez-Vidal, A., Guitton-Sert, L., Cadoret, J.C., Drac, M., Schwob, E., Baldacci, G., Cazaux, C., and Hoffmann, J.S. (2014). A role for DNA polymerase θ in the timing of DNA replication. *Nat. Commun.* 5, 4285. <https://doi.org/10.1038/ncomms5285>.
26. Shima, N., Munroe, R.J., and Schimenti, J.C. (2004). The mouse genomic instability mutation chaos1 is an allele of Polq that exhibits genetic interaction with Atm. *Mol. Cell Biol.* 24, 10381–10389. <https://doi.org/10.1128/MCB.24.23.10381-10389.2004>.
27. Belan, O., Barroso, C., Kaczmarczyk, A., Anand, R., Federico, S., O'Reilly, N., Newton, M.D., Maeots, E., Enchev, R.I., Martinez-Perez, E., et al. (2021). Single-molecule analysis reveals cooperative stimulation of Rad51 filament nucleation and growth by mediator proteins. *Mol. Cell* 81, 1058.e7–1073.e7. <https://doi.org/10.1016/j.molcel.2020.12.020>.
28. Feng, W., Simpson, D.A., Carvajal-Garcia, J., Price, B.A., Kumar, R.J., Mose, L.E., Wood, R.D., Rashid, N., Purvis, J.E., Parker, J.S., et al. (2019). Genetic determinants of cellular addiction to DNA polymerase theta. *Nat. Commun.* 10, 4286. <https://doi.org/10.1038/s41467-019-12234-1>.
29. Petermann, E., Orta, M.L., Issaeva, N., Schultz, N., and Helleday, T. (2010). Hydroxyurea-stalled replication forks become progressively inactivated and require two different RAD51-mediated pathways for restart and repair. *Mol. Cell* 37, 492–502. <https://doi.org/10.1016/j.molcel.2010.01.021>.

30. Hewitt, G., Borel, V., Segura-Bayona, S., Takaki, T., Ruis, P., Bellelli, R., Lehmann, L.C., Sommerova, L., Vancevska, A., Tomas-Loba, A., et al. (2021). Defective ALC1 nucleosome remodeling confers PARPi sensitization and synthetic lethality with HRD. *Mol. Cell* 81, 767–783.e11. <https://doi.org/10.1016/j.molcel.2020.12.006>.
31. Hashimoto, Y., Ray Chaudhuri, A., Lopes, M., and Costanzo, V. (2010). Rad51 protects nascent DNA from Mre11-dependent degradation and promotes continuous DNA synthesis. *Nat. Struct. Mol. Biol.* 17, 1305–1311. <https://doi.org/10.1038/nsmb.1927>.
32. Verma, P., Zhou, Y., Cao, Z., Deraska, P.V., Deb, M., Arai, E., Li, W., Shao, Y., Puentes, L., Li, Y., et al. (2021). ALC1 links chromatin accessibility to PARP inhibitor response in homologous recombination-deficient cells. *Nat. Cell Biol.* 23, 160–171. <https://doi.org/10.1038/s41556-020-00624-3>.
33. Quinet, A., Carvajal-Maldonado, D., Lemaçon, D., and Vindigni, A. (2017). DNA fiber analysis: mind the gap! *Methods Enzymol.* 591, 55–82. <https://doi.org/10.1016/bs.mie.2017.03.019>.
34. Chapman, J.R., Barral, P., Vannier, J.B., Borel, V., Steger, M., Tomas-Loba, A., Sartori, A.A., Adams, I.R., Batista, F.D., and Boulton, S.J. (2013). RIF1 is essential for 53BP1-dependent nonhomologous end joining and suppression of DNA double-strand break resection. *Mol. Cell* 49, 858–871. <https://doi.org/10.1016/j.molcel.2013.01.002>.
35. Zimmermann, M., Lottersberger, F., Buonomo, S.B., Sfeir, A., and de Lange, T. (2013). 53BP1 regulates DSB repair using Rif1 to control 5' end resection. *Science* 339, 700–704. <https://doi.org/10.1126/science.1231573>.
36. Di Virgilio, M., Callen, E., Yamane, A., Zhang, W., Jankovic, M., Gittlin, A.D., Feldhahn, N., Resch, W., Oliveira, T.Y., Chait, B.T., et al. (2013). Rif1 prevents resection of DNA breaks and promotes immunoglobulin class switching. *Science* 339, 711–715. <https://doi.org/10.1126/science.1230624>.
37. Nacson, J., Kraus, J.J., Bernhardt, A.J., Clausen, E., Feng, W., Wang, Y., Nicolas, E., Cai, K.Q., Tricarico, R., Hua, X., et al. (2018). BRCA1 mutation-specific responses to 53BP1 loss-induced homologous recombination and PARP inhibitor resistance. *Cell Rep.* 24, 3513–3527.e7. <https://doi.org/10.1016/j.celrep.2018.08.086>.
38. Zellweger, R., Dalcher, D., Mutreja, K., Berti, M., Schmid, J.A., Herrador, R., Vindigni, A., and Lopes, M. (2015). Rad51-mediated replication fork reversal is a global response to genotoxic treatments in human cells. *J. Cell Biol.* 208, 563–579. <https://doi.org/10.1083/jcb.201406099>.
39. Guo, E., Ishii, Y., Mueller, J., Srivatsan, A., Gahman, T., Putnam, C.D., Wang, J.Y.J., and Kolodner, R.D. (2020). FEN1 endonuclease as a therapeutic target for human cancers with defects in homologous recombination. *Proc. Natl. Acad. Sci. USA* 117, 19415–19424. <https://doi.org/10.1073/pnas.2009237117>.
40. Guillian, T.A., and Yeeles, J.T.P. (2020). Reconstitution of translesion synthesis reveals a mechanism of eukaryotic DNA replication restart. *Nat. Struct. Mol. Biol.* 27, 450–460. <https://doi.org/10.1038/s41594-020-0418-4>.
41. Belan, O., Moore, G., Kaczmarczyk, A., Newton, M.D., Anand, R., Boulton, S.J., and Rueda, D.S. (2021). Generation of versatile ss-dsDNA hybrid substrates for single-molecule analysis. *Star Protoc.* 2, 100588. <https://doi.org/10.1016/j.xpro.2021.100588>.
42. Schaub, J.M., Soniat, M.M., and Finkelstein, I.J. (2022). Polymerase theta-helicase promotes end joining by stripping single-stranded DNA-binding proteins and bridging DNA ends. *Nucleic Acids Res.* 50, 3911–3921. <https://doi.org/10.1093/nar/gkac119>.
43. Koole, W., van Schendel, R., Karambelas, A.E., van Heteren, J.T., Okihara, K.L., and Tijsterman, M. (2014). A polymerase theta-dependent repair pathway suppresses extensive genomic instability at endogenous G4 DNA sites. *Nat. Commun.* 5, 3216. <https://doi.org/10.1038/ncomms4216>.
44. Hogg, M., Seki, M., Wood, R.D., Doublé, S., and Wallace, S.S. (2011). Lesion bypass activity of DNA polymerase θ (POLQ) is an intrinsic property of the pol domain and depends on unique sequence inserts. *J. Mol. Biol.* 405, 642–652. <https://doi.org/10.1016/j.jmb.2010.10.041>.
45. Volkova, N.V., Meier, B., González-Huici, V., Bertolini, S., Gonzalez, S., Vöhringer, H., Abascal, F., Martincorena, I., Campbell, P.J., Gartner, A., and Gerstung, M. (2020). Mutational signatures are jointly shaped by DNA damage and repair. *Nat. Commun.* 11, 2169. <https://doi.org/10.1038/s41467-020-15912-7>.
46. Yoon, J.H., McArthur, M.J., Park, J., Basu, D., Wakamiya, M., Prakash, L., and Prakash, S. (2019). Error-prone replication through UV lesions by DNA polymerase θ protects against skin cancers. *Cell* 176, 1295–1309.e15. <https://doi.org/10.1016/j.cell.2019.01.023>.
47. Tagliatela, A., Leuzzi, G., Sannino, V., Cuella-Martin, R., Huang, J.W., Wu-Baer, F., Baer, R., Costanzo, V., and Ciccio, A. (2021). REV1-Pol ζ maintains the viability of homologous recombination-deficient cancer cells through mutagenic repair of PRIMPOL-dependent ssDNA gaps. *Mol. Cell* 81, 4008–4025.e7. <https://doi.org/10.1016/j.molcel.2021.08.016>.
48. Kent, T., Chandramouly, G., McDevitt, S.M., Ozdemir, A.Y., and Pomerantz, R.T. (2015). Mechanism of microhomology-mediated end-joining promoted by human DNA polymerase θ . *Nat. Struct. Mol. Biol.* 22, 230–237. <https://doi.org/10.1038/nsmb.2961>.
49. Zahn, K.E., Averill, A.M., Aller, P., Wood, R.D., and Doublé, S. (2015). Human DNA polymerase θ grasps the primer terminus to mediate DNA repair. *Nat. Struct. Mol. Biol.* 22, 304–311. <https://doi.org/10.1038/nsmb.2993>.
50. Yu, A.M., and McVey, M. (2010). Synthesis-dependent microhomology-mediated end joining accounts for multiple types of repair junctions. *Nucleic Acids Res.* 38, 5706–5717. <https://doi.org/10.1093/nar/gkq379>.
51. Muzzini, D.M., Plevani, P., Boulton, S.J., Cassata, G., and Marini, F. (2008). *Caenorhabditis elegans* POLQ-1 and HEL-308 function in two distinct DNA interstrand cross-link repair pathways. *DNA Repair (Amst)* 7, 941–950. <https://doi.org/10.1016/j.dnarep.2008.03.021>.
52. Hussmann, J.A., Ling, J., Ravisankar, P., Yan, J., Cirincione, A., Xu, A., Simpson, D., Yang, D., Bothmer, A., Cotta-Ramusino, C., et al. (2021). Mapping the genetic landscape of DNA double-strand break repair. *Cell* 184, 5653–5669.e25. <https://doi.org/10.1016/j.cell.2021.10.002>.
53. Gallina, I., Hendriks, I.A., Hoffmann, S., Larsen, N.B., Johansen, J., Colding-Christensen, C.S., Schubert, L., Sellés-Baiget, S., Fábrián, Z., Kühbacher, U., et al. (2021). The ubiquitin ligase RFW3 is required for translesion DNA synthesis. *Mol. Cell* 81, 442.e9–458.e9. <https://doi.org/10.1016/j.molcel.2020.11.029>.
54. ClinicalTrials.gov (2021). A study of ART4215 for the treatment of advanced or metastatic solid tumors. <https://clinicaltrials.gov/ct2/show/NCT04991480>.
55. Llorens-Agost, M., Ensminger, M., Le, H.P., Gawai, A., Liu, J., Cruz-García, A., Bhetawal, S., Wood, R.D., Heyer, W.D., and Löbrich, M. (2021). POL θ -mediated end joining is restricted by RAD52 and BRCA2 until the onset of mitosis. *Nat. Cell Biol.* 23, 1095–1104. <https://doi.org/10.1038/s41556-021-00764-0>.
56. Carvajal-García, J., Crown, K.N., Ramsden, D.A., and Sekelsky, J. (2021). DNA polymerase theta suppresses mitotic crossing over. *PLoS Genet.* 17, e1009267. <https://doi.org/10.1371/journal.pgen.1009267>.
57. van Bostelen, I., van Schendel, R., Romeijn, R., and Tijsterman, M. (2020). Translesion synthesis polymerases are dispensable for *C. elegans* reproduction but suppress genome scarring by polymerase theta-mediated end joining. *PLoS Genet.* 16, e1008759. <https://doi.org/10.1371/journal.pgen.1008759>.
58. Fugger, K., Bajrami, I., Silva Dos Santos, M., Young, S.J., Kunzelmann, S., Kelly, G., Hewitt, G., Patel, H., Goldstone, R., Carell, T., et al. (2021). Targeting the nucleotide salvage factor DNPH1 sensitizes BRCA-deficient

- p>cells to PARP inhibitors.
- Science*
- 372, 156–165.
- <https://doi.org/10.1126/science.abb4542>
- .
59. Langevin, F., Crossan, G.P., Rosado, I.V., Arends, M.J., and Patel, K.J. (2011). Fancd2 counteracts the toxic effects of naturally produced aldehydes in mice. *Nature* 475, 53–58. <https://doi.org/10.1038/nature10192>.
60. Zimmer, J., Tacconi, E.M.C., Folio, C., Badie, S., Porru, M., Klare, K., Tumiat, M., Markkanen, E., Halder, S., Ryan, A., et al. (2016). Targeting BRCA1 and BRCA2 deficiencies with G-quadruplex-interacting compounds. *Mol. Cell* 61, 449–460. <https://doi.org/10.1016/j.molcel.2015.12.004>.
61. van Schendel, R., Romeijn, R., Buijs, H., and Tijsterman, M. (2021). Preservation of lagging strand integrity at sites of stalled replication by Pol alpha-primase and 9-1-1 complex. *Sci. Adv.* 7, eabf2278. <https://doi.org/10.1126/sciadv.abf2278>.
62. Daboussi, F., Courbet, S., Benhamou, S., Kannouche, P., Zdzienicka, M.Z., Debatisse, M., and Lopez, B.S. (2008). A homologous recombination defect affects replication-fork progression in mammalian cells. *J. Cell Sci.* 121, 162–166. <https://doi.org/10.1242/jcs.010330>.
63. Stringer, B.W., Day, B.W., D’Souza, R.C.J., Jamieson, P.R., Ensbey, K.S., Bruce, Z.C., Lim, Y.C., Goasdoué, K., Offenhäuser, C., Akgül, S., et al. (2019). A reference collection of patient-derived cell line and xenograft models of proneural, classical and mesenchymal glioblastoma. *Sci. Rep.* 9, 4902. <https://doi.org/10.1038/s41598-019-41277-z>.
64. Jackson, D.A., and Pombo, A. (1998). Replicon clusters are stable units of chromosome structure: evidence that nuclear organization contributes to the efficient activation and propagation of S phase in human cells. *J. Cell Biol.* 140, 1285–1295. <https://doi.org/10.1083/jcb.140.6.1285>.
65. Anand, R., Buechelmaier, E., Belan, O., Newton, M., Vancevska, A., Kaczmarczyk, A., Takaki, T., Rueda, D.S., Powell, S.N., and Boulton, S.J. (2022). HELQ is a dual-function DSB repair enzyme modulated by RPA and RAD51. *Nature* 601, 268–273. <https://doi.org/10.1038/s41586-021-04261-0>.

STAR★METHODS

KEY RESOURCES TABLE

REAGENT or RESOURCE	SOURCE	IDENTIFIER
Antibodies		
anti-BRCA2	Millipore	Cat#OP95; RRID: AB_206776
anti-Histone H3	Abcam	Cat#ab10799; RRID: AB_470239
anti-53BP1	Bethyl	Cat#A300-272A; RRID: AB_185520
anti-RAD51	Millipore	Cat#ABE257; RRID: AB_10850319
anti-PCNA	Santa Cruz	Cat#CS-56; RRID: AB_628110
anti-POLQ	Dr. Jean-Sébastien Hoffman	N/A
Goat anti-Mouse Immunoglobulins/HRP	Agilent-Dako	Cat#P0447; RRID:AB_2617137
Swine anti-Rabbit Immunoglobulins/HRP	Agilent-Dako	Cat#P0399; RRID:AB_2617141
rat monoclonal anti-BrdU	Abcam	Cat#ab6326; RRID: AB_305426
mouse monoclonal anti-BrdU	Becton Dickinson	Cat#347580; RRID: AB_10015219
goat anti-Rat IgG (H+L), Alexa Fluor 594 conjugated	Thermo Fisher	Cat#A-11007; RRID: AB_10561522
rabbit anti-Mouse IgG (H+L), Alexa Fluor488 conjugated	Thermo Fisher	Cat#A-11059; RRID: AB_2534106
Bacterial and virus strains		
<i>E. coli</i> BL21(DE3)	NEB	Cat#C25271
<i>E. coli</i> DH5alpha	NEB	Cat#C2987H
<i>E. coli</i> Rosetta(DE3)pLysS	Merck	Cat#70956-3
Chemicals, peptides, and recombinant proteins		
Ampicillin, Sodium Salt	Merck	Cat#171254
Chloramphenicol	Merck	Cat#220551
IPTG, Dioxane-Free, High Purity	Merck	Cat#420322
Sodium hypochlorite	Merck	Cat#XX0637
Sodium thiosulfate	Merck	Cat#106512
PLURONIC F-127	Merck	Cat#P2443-250G
Albumin from bovine serum	Sigma-Aldrich	Cat#A7030
HiTrap Heparin HP 1 mL column	Merck	Cat#GE17-0407-01
Streptavidin-coated polystyrene particles 0.5% w/v	SpheroTech	Cat#SVP-40-5
Ni-NTA agarose resin	Qiagen	Cat#30210
Lambda DNA	Thermo Fisher	Cat#SD0011
CoA Alexa 555 conjugate	Crick Peptide Chemistry STP	N/A
CoA Alexa 647 conjugate	Crick Peptide Chemistry STP	N/A
CoA Alexa 488 conjugate	Crick Peptide Chemistry STP	N/A
POLQ PD	This study	N/A
POLQ PD-ybbr-Alexa 488	This study	N/A
POLQ PD-ybbr-Alexa 555	This study	N/A
POLQ PD-ybbr-Alexa 647	This study	N/A
POLQ HD	This study	N/A
LIG1	This study	N/A
FEN1	This study	N/A
Sfp phosphopantetheinyl transferase	This study	N/A
Klenow Fragment (exo -)	NEB	Cat#M0212L
RPA-EGFP	This study	N/A

(Continued on next page)

Continued

REAGENT or RESOURCE	SOURCE	IDENTIFIER
his ₆ -SUMO protease	Dr. Peter Cherepanov	N/A
T4 Polynucleotide Kinase	NEB	Cat#M0201S
T4 DNA Ligase	NEB	Cat#M0202S
T4 DNA Ligase Reaction Buffer	NEB	Cat#B0202S
SYTOX Orange Nucleic Acid Stain	Thermo Fisher	Cat#S11368
S. p. Cas9 nuclease V3	IDT	Cat#1081059
S. p. Cas9 D10A nickase	IDT	Cat#1081062
DAPI	Life Technology	Cat#D21490
Doxycycline	Sigma-Aldrich	Cat#M0503-5X2MG
Blasticidin	Thermo Fisher	Cat#A1113903
Hygromycin B	Thermo Fisher	Cat#10687010
Zeocin	ThermoFisher	Cat#R25005
Puromycin	ThermoFisher	Cat#A1113803
Lipofectamine 2000	Thermo Fisher	Cat#11668019
Talazoparib	Selleck Chemicals	Cat#S7048
EDTA-free Complete protease inhibitor cocktail	Roche	Cat#COEDTAF-RO
PhosSTOP phosphatase inhibitor cocktail	Roche	Cat#PHOSS-RO
4x NuPAGE LDS sample buffer	Thermo Fisher	Cat#NP0008
ProLong Gold antifade with DAPI	Thermo Fisher	Cat#P36931
Lipofectamine RNAiMAX	Invitrogen	Cat#13778150
Olaparib	Selleck Chemicals	Cat#S1060
Clarity Western ECL	Bio-Rad	Cat#1705061
Clarity Max Western ECL	Bio-Rad	Cat#1705062
Benzonase Nuclease	Millipore-Merck	Cat#E1014
Diethylnitrosamine	Sigma-Aldrich	Cat#N0756
CldU	Sigma-Aldrich	Cat#C6891
JH-RE-06	Selleckchem	Cat#S8850
ART558	Artios Pharma	N/A
IdU	Sigma-Aldrich	Cat#I7125
EdU	Thermo Fisher	Cat#A10044
S1 nuclease	Invitrogen	Cat#18001016

Critical commercial assays

QIAquick PCR Purification Kit	Qiagen	Cat#28104
CellTiter-Glo	Promega	Cat#G8462
Q5 Site-Directed Mutagenesis Kit	New England BioLabs	Cat#E0554
Nano-Glo Dual-Luciferase Reporter Assay System	Promega	Cat#N1610
Click-iT EdU Imaging Kit	Life Technology	Cat#C10340

Deposited data

Original images with cropped areas marked	This paper	Mendeley Data: https://doi.org/10.17632/pxmh4jsb54.1
Original code used for analysis of single-molecule data	This paper	Zenodo: https://doi.org/10.5281/zenodo.7293678

Experimental models

eHAP iCAS9 clone #3	Hewitt et al. ³⁰	N/A
eHAP iCAS9 POLQ ^{-/-} clone #4	This study	N/A
eHAP iCAS9 POLQ ^{-/-} clone #6	This study	N/A
DLD-1 BRCA2 ^{+/+}	Horizon Discovery	Cat#HD 105-007

(Continued on next page)

Continued

REAGENT or RESOURCE	SOURCE	IDENTIFIER
DLD-1 BRCA2 ^{−/−}	Horizon Discovery	Cat#HD 105-007
SUM149PT (BRCA1 mutant)	BiolVT	Cat#HUMANSUM-0003004
SUM149PT revertant	Dr. Graeme Hewitt	N/A
SUM149PT pooled SHLD2 KO	Artios Pharma, this study	N/A
SUM149PT pooled 53BP1 KO	Artios Pharma, this study	N/A
SUM149PT pooled RIF1 KO	Artios Pharma, this study	N/A
SUM149PT pooled REV7 KO	Artios Pharma, this study	N/A

Recombinant DNA

pET151d/t-his-SUMO-POLQ PD	This study	N/A
pET151d/t-his-SUMO-POLQ PD-ybbr	This study	N/A
pET151d/t-his-SUMO-POLQ HD	This study	N/A
pET151d/t-his-SUMO-FEN1	This study	N/A
pET151d/t-his-SUMO-LIG1	This study	N/A
pET-29-Sfp	Dr. Meindert Lamers	N/A
phRPA-EGFP	Dr. Mauro Modesti	N/A
POLQ-Lenti-sgRNA-Puro	This study	N/A
NanoLuciferase TMEJ repair reporter substrate	Artios Pharma	N/A

Software and algorithms

GraphPad Prism 9	Graphpad	https://www.graphpad.com/scientific-software/prism/
Fiji	Open source	https://imagej.net/Fiji
Matlab R2018b (9.5.0)	MathWorks	https://uk.mathworks.com
Lumicks Pylake	Python package from Lumicks	https://lumicks-pylake.readthedocs.io/en/latest/index.html#
CellProfiler ver. 4.2.1	Broad Institute	https://cellprofiler.org

Other

C-trap optical trapping and confocal microscopy setup	Lumicks	N/A
---	---------	-----

RESOURCE AVAILABILITY

Lead contact

Further information and requests for resources and reagents should be directed to and will be fulfilled by the Lead Contact, Simon J. Boulton (simon.boulton@crick.ac.uk).

Materials availability

Plasmids, recombinant proteins, DNA substrates and cell lines are available without restriction upon requests, which should be directed to the Lead Contact, Simon J Boulton (simon.boulton@crick.ac.uk).

Data and code availability

Immunofluorescence images, scanned gels, scanned clonogenic wells, original wester blot data and all other uncropped original images have been deposited at Mendeley at <https://doi.org/10.17632/pxmh4jsb54.1> and are publicly available as of the date of publication. The DOI is listed in the key resources table. Microscopy data reported in this paper will be shared by the lead contact upon request. The original code used to process single-molecule data has been deposited at Zenodo at <https://doi.org/10.5281/zenodo.7293678> and is publicly available as of the date of publication. DOIs are listed in the key resources table. Any additional information required to reanalyze the data reported in this paper is available from the lead contact upon request.

EXPERIMENTAL MODEL AND SUBJECT DETAILS

Bacterial strains

DH5 α *E. coli* strain (genotype: fhuA2 Δ (argF-lacZ)U169 phoA glnV44 Φ 80 Δ (lacZ)M15 gyrA96 recA1 relA1 endA1 thi-1 hsdR17) was transformed with protein expression plasmids ([key resources table](#)) and grown in Luria Broth at 37 °C in the presence of 50 μ g/ml kanamycin. BL21(DE3) *E. coli* strain (genotype: fhuA2 [lon] ompT gal (λ DE3) [dcm] Δ hsdS; λ DE3 = λ sBamHI Δ EcoRI-B int::[lacI::PlacUV5::T7 gene1] i21 Δ nin5) was transformed with protein expression plasmids ([key resources table](#)) and grown in Luria Broth at 37 °C in the presence of with ampicillin (100 μ g/ml) and induced by 0.2 mM IPTG at 18 °C for 16 h. Rosetta(DE3)pLysS *E. coli* strain (genotype: F⁻ ompT hsdS_B(r_B⁻ m_B⁻) gal dcm (DE3) pLysSRARE (Cam^R)) was transformed with protein expression plasmids ([key resources table](#)) and grown in Luria Broth at 37 °C in the presence of with ampicillin (100 μ g/ml) and chloramphenicol (34 μ g/ml) and induced by 1 mM IPTG at 15 °C for 16 h.

Cell lines

The human haploid chronic myeloid leukemia cell line, eHAP,³⁰ was purchased from Horizon Discovery (#C669) and maintained in IMDM medium (GIBCO/Thermo Fisher) supplemented with 10% FBS and Pen/Strep. In the study, we used stable diploid eHAP cells. SUM149PT (BioIVT HUMANSUM-0003004) cells were purchased from BioIVT and routinely maintained in Ham's F-12 Medium (Gibco, 11765054) supplemented with 5% foetal bovine serum (Pan-Biotech, P30-3031), 10 mM HEPES (Sigma-Aldrich, H0887), 1 μ g/mL Hydrocortisone (Sigma-Aldrich, H0135-1MG), and 5 μ g/mL Insulin (Sigma-Aldrich, I9278 - 5mL). Cells were grown at their optimal growth density and maintained at 37 °C in a humidified atmosphere containing 5% carbon dioxide (CO₂). The 53BP1-RIF1-shiledin complex knockout (KO) cell lines derived from SUM149PT were generated as described in [method details](#), and routinely maintained in Ham's F-12 Medium (Gibco, 11765054) supplemented with 5% foetal bovine serum (Pan-Biotech, P30-3031), 10 mM HEPES (Sigma-Aldrich, H0887), 1 μ g/mL Hydrocortisone (Sigma-Aldrich, H0135-1MG), and 5 μ g/mL Insulin (Sigma-Aldrich, I9278 - 5mL). SUM149PT revertant cell line were provided by Dr. Graeme Hewitt, who received the cell line as a kind gift from Prof. Chris Lord (ICR London), and maintained in Ham's F-12 Medium (Gibco, 11765054) supplemented with 5% foetal bovine serum (Pan-Biotech, P30-3031), 10 mM HEPES (Sigma-Aldrich, H0887), 1 μ g/mL Hydrocortisone (Sigma-Aldrich, H0135-1MG), and 5 μ g/mL Insulin (Sigma-Aldrich, I9278 - 5mL).

METHOD DETAILS

Generation of CRISPR knockout cell lines

CRISPR gRNA against POLQ with the target sequence GACTTGTCAGGCCACTAGTG was cloned into lenti-sgRNA-Puro (Addgene # 104990)⁶³ using oligos F:CACCGGACTTGTCAGGCCACTAGTG and R: AAACCACTAGTGCCCTGACAAAGTCC. eHAP iCas9 cells³⁰ were seeded 400,000/well of a six well plate and cells were transfected 24 h later with 2 μ g POLQ-Lenti-sgRNA-Puro in media containing 1 μ g/ml Dox to induce Cas9 expression. 36 h following transfection cells were selected in media containing 0.4 μ g/ml puromycin and 1 μ g/ml Dox to maintain Cas9 expression for 48 h. Cells were then seeded at limiting dilution and grown for 5 days to allow single colonies to form. Single clones were isolated and expanded clones were screened for loss of TMEJ using the nanoLuc reporter assay published in Zatreanu et al.¹³ POLQ knockout was then confirmed by Western blotting. To generate 53BP1-RIF1-shiledin complex knockout (KO) cell lines SUM149PT cells were co-transfected with Edit-R Cas9 Nuclease protein NLS (Horizon Discovery, CAS11200), Edit-R CRISPR-Cas9 Synthetic tracrRNA (Horizon Discovery, U-002005-05), and Edit-R Human crRNA targeting the gene of interest using DharmaFECT Duo Transfection Reagent (Horizon Discovery, T-2010-01, [Table S1](#)). Pool of edited cells was then cultured in the presence of 2 μ M Olaparib (Selleck Chemicals, S1060) or 100 nM Talazoparib (Selleck Chemicals, S7048) to select KO cells. Gene KO was validated by western blotting, and/or phenotypic characterisation when possible.

RNA interference

BRCA1 was targeted with 25 nM siGENOME smart-pool (M-003461-02). BRCA2 was targeted with 25 nM siGENOME smart-pool (M-003462-01). siRNA oligonucleotides were transfected in Opti-MEM reduced-serum medium using RNAiMAX (Life Technologies/Thermo Fisher). Following siRNA transfection, cells were seeded either for survival assays (24 h post transfection) or for immunofluorescence and DNA fibre analysis (48 h post transfection). If cells were treated with genotoxin. The treatment was typically performed 24h after the transfection and 24 before the experiment.

Drug treatment and cell survival analysis using colony formation assay and CellTiter-Glo assay

POLQ +/+ and POLQ -/- eHAPs were seeded at the density of 200 cells per well in a 96 well plate. For POLQ -/- eHAPs following BRCA2-depletion, 800 cells were plated per well. Cells were treated with indicated dose of drug for 24 h following plating and grown for 5 more days. CellTiter-Glo assay (Promega) was performed as described in manufacturer's instruction. Luminescence was measured using CLARIOstar Plus plate reader (BMG Labtech). Luminescence signal in treated wells was normalized to untreated POLQ +/+ eHAPs or untreated wells for each genotype. Data were fitted with sigmoid fit in GraphPad Prism 7.0. Clonogenic survival analysis for eHAP cells was performed as described previously.³⁰ For clonogenic

survival of SUM149PT cells, cells were seeded onto 12-well (VWR, 734-0055) or 24-well plates (VWR, 734-0056), and, 24-hours later, treated with media containing a range of ART558 and/or Olaparib (Selleck Chemicals, S1060) concentrations. After 11- or 13-days incubation at 37 °C with 5% FBS, medium was removed, cells were fixed with 70% ethanol (VWR, 20821.33), and stained with 0.4% crystal violet (Sigma-Aldrich, V5265-500mL). Pictures were acquired using the GelCount (Oxford Opttronix Ltd) colony counter, colonies were solubilised using 10% acetic acid (VWR, 20103.330), and absorbance at 590 nm was read using the CLARIOstar® (BMG Labtech) plate reader. Survival for each compound was plotted as a percentage of survival normalised against wells treated with vehicle only, either DMSO (Apollo Scientific, BID1200-250mL) (monotherapy) or 5 μ M ART558 (combination).

Western blotting

Cells were treated with indicated concentration of drug for 24 hours. Followed by harvest and processing using subcellular protein fractionation kit (Thermo Fisher, cat. n. 78840) according to manufacturer's instructions. Each fraction was mixed with equivalent volume of 2x Laemmli buffer, incubated for 5-10 min at 99 °C and loaded onto 4-12% NUPAGE Bis-Tris gels for SDS-PAGE analysis. Gels were run at 150 V for 90 min, alongside a SeeBlue Plus2 pre-stained protein ladder (Thermo Fisher). Proteins were transferred to 0.2 μ m nitrocellulose membranes in transfer buffer (25 mM Tris-HCl pH 7.5, 190 mM glycine, 20% methanol) at 0.4 A for 60 min at 4 °C. Membranes were incubated with blocking solution (3% BSA, 0.1 % Tween20 in PBS) for 1 hour with agitation at 25 °C. Primary antibodies (in blocking solution) were incubated with the membrane overnight at 4 °C with mild agitation (α POLQ was a kind gift from Dr. Jean-Sébastien Hoffmann²⁵; α BRCA2 – Millipore, Cat#OP95, AB_206776; α H3 – Abcam, Cat#ab10799, RRID:AB_470239). Membranes were washed 3 times for 10 minutes with 0.1 % Tween20 in PBS and subsequently incubated with HRP-conjugated secondary antibodies (goat anti-Mouse Immunoglobulins/HRP - Agilent-Dako, Cat#P0447, RRID:AB_2617137; swine anti-Rabbit Immunoglobulins/HRP- Agilent-Dako, Cat#P0399, RRID:AB_2617141) in blocking solution for 1 h at 4 °C. Membranes were washed further 3 times for 10 min each wash with 0.1 % Tween20 in PBS. Proteins were detected using ChemiDoc imaging system (Bio-Rad).

Indirect immunofluorescence

POLQ +/- and POLQ -/- eHAPs were washed in PBS and treated with pre-extraction buffer (10 mM HEPES pH 7, 50 mM NaCl, 300 mM sucrose, 3 mM MgCl₂, 5 mM EDTA, and 0.5% Triton X-100) for 7 min on ice, washed with PBS and then fixed with 4% paraformaldehyde in PBS for 15 min at 25 °C. Coverslips with cells were washed 3 times for 5 min with PBS at 25 °C and stored at 4 °C. Coverslips with fixed cells were then permeabilized with detergent solution (0.1% Triton X-100, 0.02% SDS in PBS), washed with PBS, incubated with 2% BSA in PBS for 10 min and blocked with blocking solution (10% normal goat serum (Sigma Aldrich, cat. n. G9023-10mL), 2% BSA in PBS). Primary antibodies (α RPA pS33 – Bethyl, Cat#A300-246A, RRID:AB_2180847; α 53BP1 – Bethyl, Cat#A300-272A, RRID:AB_185520; α RAD51 – Millipore, Cat#ABE257, RRID:AB_10850319) were added in blocking solution and incubated with the coverslips for 1 h at 25 °C. Coverslips were then washed three times for 4 min each with 2% BSA in PBS. Fluorescent secondary antibodies were added, and samples were incubated for 45 min at 25 °C. Coverslips were washed three times for 4 min each with 2% BSA in PBS, dripped in water, allowed to dry and mounted onto microscope slides with ProLong™ Gold Antifade with DAPI (Invitrogen). Images were acquired using a Zeiss AxioImager M1, equipped with a Hamamatsu digital camera and the Velocity software (Perkin Elmer). Images were processed in Fiji and foci were counted automatically using customized pipeline based on 'speckle' template in CellProfiler. For native CldU staining cells were incubated for 48h with 10 μ M CldU. Next, CldU was washed out and cells were treated with 0.5 μ M of Olaparib for 2h. This way treated cells were subjected to pre-extraction with the use of CSK buffer (10 mM Pipes, pH 7.0, 100 mM NaCl, 300 mM sucrose, and 3 mM MgCl₂, 0.5% Triton X-100) on ice for 3min. Subsequently cells were washed with cold PBS and fixed with cold 4% PFA for 10 min at 25 °C. Next, cells were permeabilised with cold Methanol for 5 min, washed with PBS and blocked with 5% BSA solution in PBS for 1 h. This was followed by the incubation with primary antibodies: BrdU (Abcam 6326; 1:1000) and PCNA (cs-56; 1:300) for 1h. Next, cells were incubated with appropriate secondary antibodies, counterstained with DAPI and mounted with the use of Moviol.

Extrachromosomal luminescence-based MMEJ assay

The NanoLuciferase MMEJ repair reporter assay was performed as described previously.¹³ Briefly, POLQ +/- eHAP cells and POLQ -/- eHAP cells were trypsinised, washed, and resuspended in fresh media. After counting, cells were transfected with Firefly and NanoLuciferase containing plasmids for physical end-joining efficiency estimation (NanoLuciferase) and transfection efficiency normalization (Firefly). Firefly and NanoLuciferase levels were detected using the Nano-Glo Dual-Luciferase Reporter Assay system (Promega) as per the manufacturer's instructions, and luminescence was measured with a Clariostar plate reader (BMG Labtech), using the manufacturer's protocols 'FireFly' and 'NanoLuciferase'. In each experimental well the NanoLuciferase signal was normalised to the Firefly signal, which served as a measure of both cell density and transfection efficiency and then normalised to the eHAP wt control.

DNA fiber analysis with S1 nuclease digestion

The experiments were performed similarly as described previously.³³ Cells were seeded at places at appropriate confluency 24 hours before the experiment or 24 hours before drug treatment. In case of drug treatment, cells were treated for 24 hours the day before the experiment with indicated dose of olaparib. On the day of the experiment, cells were pulse labelled with 25 μ M

CldU and 250 μ M IdU (15 μ M CldU and 150 μ M IdU for DNA fiber analysis in SUM149PT cell lines) for indicated time period. Cells were permeabilized with CSK100 (100 mM NaCl, 10 mM HEPES, pH 7, 3 mM $MgCl_2$, 300 mM sucrose, 0.5% Triton X-100) for 7 min at room temperature, washed with cold PBS, once with S1 nuclease buffer (30 mM sodium acetate, 10 mM zinc acetate, 5% glycerol, 50 mM NaCl, pH 4.6) and incubated with 20 U/mL S1 nuclease (Invitrogen Cat #18001016) in S1 nuclease buffer for 1 h (30 min for SUM149PT cell lines) at 37 °C. After removal of S1 nuclease buffer, PDS + 0.1% BSA was added. Nuclei were then scraped and centrifuged at 7000 rpm for 5 min at 4 °C. Supernatant was then removed leaving an appropriate volume to obtain $1.0\text{--}2.0 \times 10^3$ nuclei/ μ L. Nuclei were then resuspended, and DNA spreads were prepared by spotting 2 μ L of cells on a glass slide, followed by lysis with 7 μ L (14 μ L for SUM149PT cell lines) of spreading buffer (200 mM Tris-HCl pH 7.4, 50 mM EDTA, 0.5% SDS). Slides were tilted (15° horizontal), allowing DNA to run slowly down the slide and spread well, air-dried and then fixed in methanol/acetic acid (3:1) for 10 min at 25 °C. Slides were then washed 3 times for 5 min with H_2O . DNA was denatured by 2.5 M HCl for 75 min at 25 °C, followed by washing with PBS and blocking solution (1% BSA, 0.1% Tween20 in PBS). Slides were blocked for 1 h at 25 °C in blocking solution and subsequently incubated with rat anti-bromodeoxyuridine (detects CldU, abcam, ab6326, 1:1200 dilution in blocking solution) and mouse anti-bromodeoxyuridine (detects IdU, B44, Becton Dickinson, 1:500 dilution in blocking solution) for 1 h, rinsed 3 times with PBS and washed 3 times (2, 2 and 10 min) with blocking solution and incubated with anti-rat IgG AlexaFluor 555 and anti-mouse IgG AlexaFluor 488 (both at 1:500 dilution in blocking solution, Molecular Probes) for 1.5 h. Slides were then rinsed 2 times with PBS, washed 3 times (2, 2 and 10 min) with blocking solution and rinsed again 2 times with PBS. Slides were mounted with ProLong™ Gold Antifade (Invitrogen). Images were acquired using a Zeiss Axiomager M1, equipped with a Hamamatsu digital camera and the Volocity software (Perkin Elmer). Fiber length was analyzed using Fiji. For fork speed analysis, during each independent experiment, a minimum of 200–300 fibers were measured per condition. Fork asymmetry was measured as a percentage of the length ratio of the shortest to the longest fiber of first label origin fibers. Replication fork speed (r_f) was calculated as follows:

$$r_f = \frac{l \times c_f}{\Delta t}$$

where l is length of the DNA fibre in mm and c_f is a conversion factor of 2.59 kb per μ m.⁶⁴

Protein expression and purification

POLQ PD, POLQ HD, FEN1 and LIG1 were all expressed and purified as described previously^{8,44,48} with modifications. Briefly, pET151d/t vector containing polyhistidine tag upstream of SUMO fused to N-terminus of protein of interest is transformed into BL21(DE3) competent cells. Large-scale bacterial culture is grown in LB media supplemented with ampicillin (100 μ g/ml, FEN, LIG, POLQ HD) until OD 0.7 is reached. Expression is induced by 0.2 (POLQ PD and POLQ HD) or 0.5 (FEN1 and LIG1) mM IPTG at 18 °C for 16 h (POLQ PD and POLQ HD) or 30 °C for 4 h (FEN1 and LIG1). Cells are then harvested and lysed in Lysis buffer (50 mM HEPES pH 8.0, 300 mM NaCl, 10% glycerol, 1.0% NP40, 5 mM 2- β -mercaptoethanol (BME)) supplemented with EDTA-free protease inhibitor tablets. Following sonication using Branson Sonifier 450 (large flat tip, duty cycle 50%, output control 8), the lysate was clarified by ultracentrifugation at 36 000 rpm for 45 min at 4 °C. The clarified lysate was mixed with Ni-NTA slurry (washed with Lysis buffer) for 1 h at 4 °C with gentle rotation. Samples are passed through 30 ml Biorad protein purification columns and washed with NiNTA W1 buffer (50 mM HEPES pH 8.0, 300 mM NaCl, 10% glycerol, 0.01% NP40, 5 mM BME, 10 mM imidazole pH 8.0) and NiNTA W2 buffer (50 mM HEPES pH 8.0, 1000 mM NaCl, 10% glycerol, 0.01% NP40, 5 mM BME, 10 mM imidazole pH 8.0). Protein is eluted using NiNTA Elution buffer (50 mM HEPES pH 8.0, 300 mM NaCl, 10% glycerol, 0.01% NP40, 5 mM BME, 250 mM imidazole pH 8.0) and dialyzed overnight against 4 l of modified Heparin Buffer A (50 mM HEPES pH 8.0, 150 mM NaCl, 10% glycerol, 0.01% NP40, 0.1 mM EDTA, 0.5 mM DTT). Dialysed protein is then incubated with his-Ulp1 SUMO protease (22 mg/ml, 1:10 000) for 45 mins at 4 °C with gentle rotation. Cleaved his-SUMO tag is fished out by incubation with NiNTA resin pre-equilibrated with Heparin Buffer A for 30 min at 4 °C with gentle rotation. Cleaved protein is then loaded at onto 1 ml HiTrap Heparin column pre-equilibrated with Heparin Buffer A (50 mM HEPES pH 8.0, 150 mM NaCl, 10% glycerol, 0.01% NP40, 0.1 mM EDTA, 1 mM DTT) using AKTA FPLC system. Bound protein is eluted using linear gradient of 0–100 % from Heparin Buffer A to Heparin Buffer B (50 mM HEPES pH 8.0, 1000 mM NaCl, 10% glycerol, 0.01% NP40, 0.1 mM EDTA, 1 mM DTT). All fractions corresponding to UV peak are analysed by SDS-PAGE and fractions containing purest protein are pooled and concentrated using Amicon Ultra concentrators with appropriate MWCO values. Finally, protein concentration and purity is determined by Coomassie Blue staining with comparison to BSA standard. Protein is aliquoted into small aliquots and flash-frozen in liquid nitrogen.

For RPA-RFP and RPA-EGFP, expression and purification was performed as described previously⁶⁵ with minor modifications. Briefly, the modified polycistronic vector pRPA-EGFP (replication protein A-enhanced Green Fluorescent Protein) containing polyhistidine tag downstream of EGFP fused to C-terminus of RPA70 transformed into Rosetta(DE3)pLysS competent cells. Cells are grown in LB supplemented with ampicillin (100 μ g/ml) and chloramphenicol (34 μ g/ml) at 37 °C till OD of 0.5. Protein expression is then induced using 1 mM IPTG for 16 h at 15 °C. Cells are resuspended in RPA lysis buffer (20 mM Tris-HCl pH 7.5, 500 mM NaCl, 2 mM β -mercaptoethanol (BME), 5 mM imidazole pH 8.0 and 10% glycerol) supplemented with EDTA-free protease inhibitor tablets (2 tablets per 100 mL). The suspension is sonicated using a Branson Sonifier 450 (large flat tip, duty cycle 50%, output control 8). Lysate is clarified at 20 000 g for 1 h at 4 °C (Optima LE-80K Ultracentrifuge (Beckman Coulter), Ti45 rotor). Clarified lysate is incubated for 1.5 h at 4 °C with gentle rotation with Ni-NTA slurry washed with RPA lysis buffer. Ni-NTA resin is then washed with

RPA cell lysis buffer containing 10 mM imidazole and protein is eluted by RPA cell lysis buffer supplemented with 250 mM imidazole. Protein is then dialyzed against RPA buffer R-A (20 mM Tris-HCl pH 7.5, 50 mM KCl, 1 mM Dithiothreitol (DTT), 0.5 mM Ethylenediaminetetraacetic acid (EDTA) and 10% glycerol). Protein is loaded onto 1 ml Hi-Trap Heparin column pre-equilibrated with RPA buffer R-A using AKTA FPLC system. The HiTrap Heparin column is washed with 10 column volumes of RPA buffer R-A and protein is eluted using linear 0 – 100 % gradient of RPA buffer R-B (20 mM Tris-HCl pH 7.5, 500 mM KCl, 1 mM DTT, 0.5 mM EDTA and 10% glycerol). All fractions corresponding to UV peak are analysed by SDS-PAGE and fractions containing purest protein are pooled and concentrated using Amicon Ultra concentrators with appropriate MWCO values. Finally, protein concentration and purity is determined by Coomassie Blue staining with comparison to BSA standard. Protein is aliquoted into small aliquots and flash-frozen in liquid nitrogen.

Expression and purification of fluorescently labelled POLQ PD variants

pET151d/t vector containing N-terminal polyhistidine tag upstream of SUMO fused and C-terminal ybbr tag fused to POLQ PD is transformed into BL21(DE3) competent cells. Large-scale bacterial culture is grown in LB media supplemented with ampicillin (100 µg/ml, FEN, LIG, POLQ HD) until OD 0.7 is reached. Expression is induced by 0.2 mM IPTG at 18 °C for 16 h. Cells are then harvested and lysed in Lysis buffer (50 mM HEPES pH 8.0, 300 mM NaCl, 10% glycerol, 1.0% NP40, 5 mM 2-β- mercaptoethanol (BME)) supplemented with EDTA-free protease inhibitor tablets. Following sonication using Branson Sonifier 450 (large flat tip, duty cycle 50%, output control 8), the lysate was clarified by ultracentrifugation at 36 000 rpm for 45 min at 4 °C. The clarified lysate was mixed with Ni-NTA slurry (washed with Lysis buffer) for 1 h at 4 °C with gentle rotation. Samples are passed through 30 ml Biorad protein purification columns and washed with NiNTA W1 buffer (50 mM HEPES pH 8.0, 300 mM NaCl, 10% glycerol, 0.01% NP40, 5 mM BME, 10 mM imidazole pH 8.0) and NiNTA W2 buffer (50 mM HEPES pH 8.0, 1000 mM NaCl, 10% glycerol, 0.01% NP40, 5 mM BME, 10 mM imidazole pH 8.0). Protein is eluted using NiNTA Elution buffer (50 mM HEPES pH 8.0, 300 mM NaCl, 10% glycerol, 0.01% NP40, 5 mM BME, 250 mM imidazole pH 8.0) and dialyzed for 2 h against 4 l of modified Heparin Buffer A (50 mM HEPES pH 8.0, 150 mM NaCl, 10% glycerol, 0.01% NP40, 0.1 mM EDTA, 0.5 mM DTT). MgCl₂ is then added to the dialyzed protein to reach final concentration of 10 mM, together with his₆-Sfp (final concentration of 1 mM) and CoA-Alexa488 or CoA-Alexa555 or CoA-Alexa647 dyes at 2-fold molar excess over the estimated protein concentration. Proteins are labelled at 4 °C for 16 h with gentle rotation. Labelled protein is then incubated with his-Ulp1 SUMO protease (22 mg/ml, 1:10 000) for 45 mins at 4 °C with gentle rotation. Cleaved his-SUMO tag is fished out by incubation with NiNTA resin pre-equilibrated with Heparin Buffer A for 30 min at 4 °C with gentle rotation. Cleaved and labelled protein is then loaded at onto 1 ml HiTrap Heparin column pre-equilibrated with Heparin Buffer A (50 mM HEPES pH 8.0, 150 mM NaCl, 10% glycerol, 0.01% NP40, 0.1 mM EDTA, 1 mM DTT) using AKTA FPLC system. Bound protein is eluted using linear gradient of 0-100 % from Heparin Buffer A to Heparin Buffer B (50 mM HEPES pH 8.0, 1000 mM NaCl, 10% glycerol, 0.01% NP40, 0.1 mM EDTA, 1 mM DTT). All fractions corresponding to UV peak are analysed by SDS-PAGE and fractions containing purest protein are pooled and concentrated using Amicon Ultra concentrators with appropriate MWCO values. Finally, protein concentration, labelling efficiency and purity is determined by Coomassie Blue staining with comparison to BSA standard and spectrophotometry. Protein is aliquoted into small aliquots and flash-frozen in liquid nitrogen.

Oligonucleotide substrate preparation

All DNA oligonucleotides used in the *in vitro* analysis were commercially synthesized and purchased from Merck Life Sciences. To prepare various substrates used in this study, when needed, combination(s) of DNA oligonucleotides were annealed together by mixing and heating them at 95 °C for 3 min in annealing buffer (50 mM Tris-HCl (pH 7.5), 150 mM NaCl, 2 mM MgCl₂) followed by gradual cooling of the samples overnight (Table S1). The names and sequences of oligos used were as follow: oligo 1 (5' FITC- CGGA TATTTCTGATGAGTCGAAAAAT-3'), oligo 2 (5'-GAAAATAAAGGGAATAGAATAAAT-Cy5-3'), oligo 3 (5'-ATTTATTTCTATTCCTTTTATTTCTGCTTTATCAAGATAATTTTCGACTCATCAG AAATATCCG-3'), oligo 4 (5'-biotin-ATTTATTTCTATTCCTTTATTTCTGCTTTATTCATTTACTTATTTGTATTAATTTTCATCCTTTATT TATATCCTTTCTGCTTTATCAAGATAATTTTCGACTCATCAGAAATATCCG-3'), oligo 1_MM1 (5'-FITC-CGGATATTTCTGATGAGTC GAAAAAG), oligo 1_MM3 (5'-FITC-CGGATATTTCTGATGAGTCGAAAAAG), oligo 1_MM4 (5'-FITC-CGGATATTTCTGATGAGTC GAAGATG), oligo 1_MM5 (5'-FITC-CGGATATTTCTGATGAGTCGAGGATG). The combinations of oligos were annealed together to prepare g120 (oligo 1 + oligo 2 + oligo 3), g120-BT (oligo 1 + oligo 2 + oligo 4), gDNA_MM1 (oligo 1_MM1 + oligo 2 + oligo 3), gDNA_MM3 (oligo 1_MM3 + oligo 2 + oligo 3), gDNA_MM4 (oligo 1_MM4 + oligo 2 + oligo 3), gDNA_MM5 (oligo 1_MM5 + oligo 2 + oligo 3). For complete annealing, oligos were mixed in 1:1:1.2 ratios with the excess of unlabelled oligo.

DNA extension assay

Proteins were diluted from concentrated stocks into R Buffer (25 mM Tris-HCl (pH 7.5), 25 mM NaCl, 2 mM MgCl₂, 5% glycerol, 0.01% Triton-X100, 1 mM DTT) which was also used in no protein controls. gDNA substrate (30 nM) was pre-incubated with RPA (300 nM, if not indicated otherwise) in R-buffer (25 mM Tris-HCl (pH 7.5), 25 mM NaCl, 2 mM MgCl₂, 5% glycerol, 0.01% Triton-X100, 1 mM DTT) supplemented with 0.1 mg/ml BSA, 0.1 mM dNTPs (each) and 1 mM ATP for 5 min at 37 °C. POLQ PD and/or POLQ HD were then added to a final concentration that is indicated and reactions were incubated for further 20 min at 37 °C. The samples were deproteinized with 0.08% SDS and 1.5 mg/ml proteinase K for 15 min at 37 °C. Subsequently samples

were loaded onto 10% 1xTBE native PAGE gel and/or 10% UREA-TBE denaturing PAGE gel. Samples were resolved at 180 V for 45 min. Gels were imaged using Bio-Rad ChemiDoc™ MP Imaging System. Percentage of DNA extension or strand displacement was assessed using Fiji.

Gap sealing assay

Proteins were diluted from concentrated stocks into R Buffer (25 mM Tris-HCl (pH 7.5), 25 mM NaCl, 2 mM MgCl₂, 5% glycerol, 0.01% Triton-X100, 1 mM DTT) which was also used in no protein controls. gDNA substrate (30 nM) was pre-incubated with RPA (400 nM) in R10-buffer (25 mM Tris-HCl (pH 7.5), 25 mM NaCl, 10 mM MgCl₂, 5% glycerol, 0.01% Triton-X100, 1 mM DTT) supplemented with 0.1 mg/ml BSA, 0.1 mM dNTPs (each) and 1 mM ATP for 5 min at 37 °C. POLQ PD, and/or POLQ HD, and/or FEN1 and/or LIG1 were then added to a final concentration of 10 nM for POLQ PD, 64 nM for POLQ HD, 50 nM for FEN1, 12.5 nM for LIG1 were incubated for further 40 min at 37 °C. The samples were deproteinized with 0.08% SDS and 1.5 mg/ml proteinase K for 15 min at 37 °C. Subsequently samples were loaded onto 10% 1xTBE native PAGE gel and/or 10% UREA-TBE denaturing PAGE gel. Samples were resolved at 180 V for 45 min. Gels were imaged using Bio-Rad ChemiDoc™ MP Imaging System. Percentage of DNA extension or strand displacement was assessed using Fiji.

DNA capture assay

Proteins were diluted from concentrated stocks into R Buffer (25 mM Tris-HCl (pH 7.5), 25 mM NaCl, 2 mM MgCl₂, 5% glycerol, 0.01% Triton-X100, 1 mM DTT) which was also used in no protein controls. gDNA-BT substrate (30 nM) was mixed with 10 nM POLQ PD(A647) in R-buffer (25 mM Tris-HCl (pH 7.5), 25 mM NaCl, 2 mM MgCl₂, 5% glycerol, 0.01% Triton-X100, 1 mM DTT) supplemented with 0.1 mg/ml BSA, 0.1 mM dNTPs (each) and 1 mM ATP, with or without 1 mM ART558, and incubated for 10 min at 37 °C. Before incubation, 20 µl sample was taken from each reaction and mixed with 2xLaemli buffer (input). Following the incubation, 10 µl of Dynabeads M-280 (Thermo Fisher Scientific), washed twice with R-buffer, were added per 80 µl of reaction mix. Incubation for 30 min at 25 °C followed. Unbound protein sample was then taken (mixed with 2xLaemli buffer in 1:1 ratio, flow fraction) and beads were washed twice with 250 µl of R-buffer (25 mM Tris-HCl (pH 7.5), 25 mM NaCl, 2 mM MgCl₂, 5% glycerol, 0.01% Triton-X100, 1 mM DTT) supplemented with 0.1 mg/ml BSA, 0.05 mM dNTPs (each) and 1 mM ATP, with or without 1 µM ART558 for 10 min at 25 °C. Beads were then mixed with 20 µl of 2xLaemli buffer to elute bound proteins (bound fraction). 15 µl of each fraction was analysed by SDS-PAGE.

Substrate preparation for single-molecule analysis

To generate gapped I DNA, biotinylated hairpin oligonucleotides (Table S1) were annealed to I dsDNA ends and ligated. S. p. Cas9 D10A nickase (IDT) bound to guide RNAs were subsequently used to generate targeted DNA nicks. The reaction was then stored at 4 °C and directly diluted in PBS on the day of the experiment. Details on preparation of gapped I DNA can be found in the published protocol.⁴¹

DNA micromanipulation, optical trapping, and fluorescence imaging

Experiments were performed using commercially available C-trap (LUMICKS) setup. Protein channels of the microfluidics chip were first passivated with BSA (0.1% were first passivated with BSA (0.1%cs ially availablemum 500 µl of both flowed through prior to use. 4.8 µm SPHERO Streptavidin Coated polystyrene beads at 0.005% w/v were flown into the laminar flow cell, captured by trapping laser (0.14 pN/nm trap stiffness) and force calibration was performed. DNA was captured between the polystyrene beads using the laminar flow cell, stretched and held at forces above 50 pN until the strands were fully melted. The presence of ssDNA gap was verified by comparison to built-in worm-like chain model. For all the imaging conditions, DNA was held at 10 pN force. Beads and DNA were kept in PBS during the experiment, while DNA was melted in R-buffer (25 mM Tris-HCl (pH 7.5), 25 mM NaCl, 2 mM MgCl₂, 5% glycerol, 0.01% Triton-X100, 1 mM DTT) supplemented with 0.2 mg/ml BSA, 0.1 mM dNTPs (each) and 1 mM ATP in the presence or absence of 5 nM RPA-EGFP. POLQ was flowed into the system in R-buffer (25 mM Tris-HCl (pH 7.5), 25 mM NaCl, 2 mM MgCl₂, 5% glycerol, 0.01% Triton-X100, 1 mM DTT) supplemented with 0.2 mg/ml BSA, 0.1 mM dNTPs (each), 10 nM SYTOX Orange and 1 mM ATP. For confocal imaging, three excitation wavelengths were used, 488 nm for EGFP and 6-FAM, 532 nm for Cy3 and 638 nm for Cy5, with emission detected in three channels with blue filter 512/25 nm, green filter 585/75 nm and red filter 640 LP with 0.1 ms/pixel dwell-time, 100 nm pixel size. Kymographs were processed and exported using custom-written scripts in Lumics Pylake package. Extension rates in real-time experiments were then estimated in Fiji. To monitor RPA-EGFP stripping by POLQ HD, the λ gDNA4/5 construct was held at a distance corresponding to a force of 10 the λer melting and incubated for 30 s in a channel containing 5 nM RPA-EGFP in R-buffer (25 mM Tris-HCl (pH 7.5), 25 mM NaCl, 2 mM MgCl₂, 5% glycerol, 0.01% Triton-X100, 1 mM DTT) supplemented with 0.2 mg/ml BSA. Reaction was initiated by moving to channel containing 50 nM POLQ HD in R-buffer (25 mM Tris-HCl (pH 7.5), 25 mM NaCl, 2 mM MgCl₂, 5% glycerol, 0.01% Triton-X100, 1 mM DTT) supplemented with 0.2 mg/ml BSA and 1 mM ATP or ATP-γ-S. Blue laser at 5 % laser power (1.6 µW) was used for imaging with 0.1 ms/pixel dwell-time, 100 nm pixel size and 5 s inter-frame wait time. Mann-Whitney test was used to assess statistical significance of the data where appropriate. Images are presented as composites.

QUANTIFICATION AND STATISTICAL ANALYSIS

To analyse foci formation, a custom CellProfiler (ver. 4.2.1) pipeline based on 'speckle' template was used for automatic foci detection across all the images. For real-time single-molecule RPA-EGFP displacement analysis, real-time force and fluorescence data were exported from BlueLake HDF5 files and analysed using custom-written scripts in Pylake Python package. Overall fluorescent intensities were normalized to the intensity of first pixel following movement to POLQ HD-containing channel. Data were fitted with single-exponential function, $y = A_{\max} (1 - \exp(-k \cdot t))$, in GraphPad Prism 9. Helicase movement and DNA extension rates in real-time experiments were estimated in Fiji. Student t test was used to assess statistical significance of the data where appropriate. To assess statistical significance between experimental conditions, where data distribution does not follow single-gaussian, two-tailed Mann-Whitney test was used to assess statistical significance of the data. Sample size and statistical significance are indicated in the figure legend.